Title

MicroRNA miR-128 represses LINE-1 (L1) retrotransposition by down-regulating the nuclear import factor TNPO1

Journal

Journal of Biological Chemistry, 292(50)

ISSN

0021-9258

Authors

Idica, Adam
Sevrioukov, Evgueni A
Zisoulis, Dimitrios G
et al.

Publication Date

2017-12-01

DOI

10.1074/jbc.m117.807677

MicroRNA miR-128 represses LINE-1 (L1) retrotransposition by down-regulating the nuclear import factor TNPO1

Received for publication, July 25, 2017, and in revised form, September 20, 2017 Published, Papers in Press, October 3, 2017, DOI 10.1074/jbc.M117.807677

Adam Idica, Evgueni A. Sevrioukov, Dimitrios G. Zisoulis, Matthias Hamdorf, Iben Daugaard, Pavan Kadandale, and Irene M. Pedersen[1]

From the Department of Molecular Biology and Biochemistry, Francisco J. Ayala School of Biological Sciences, University of California, Irvine, California 92697

Edited by Charles E. Samuel

Repetitive elements, including LINE-1 (L1), comprise approximately half of the human genome. These elements can potentially destabilize the genome by initiating their own replication and reintegration into new sites (retrotransposition). In somatic cells, transcription of L1 elements is repressed by distinct molecular mechanisms, including DNA methylation and histone modifications, to repress transcription. Under conditions of hypomethylation (*e.g.* in tumor cells), a window of opportunity for L1 derepression arises, and additional restriction mechanisms become crucial. We recently demonstrated that the microRNA miR-128 represses L1 activity by directly binding to L1 ORF2 RNA. In this study, we tested whether miR-128 can also control L1 activity by repressing cellular proteins important for L1 retrotransposition. We found that miR-128 targets the 3′ UTR of nuclear import factor transportin 1 (TNPO1) mRNA. Manipulation of miR-128 and TNPO1 levels demonstrated that induction or depletion of TNPO1 affects L1 retrotransposition and nuclear import of an L1–ribonucleoprotein complex (using L1-encoded ORF1p as a proxy for L1–ribonucleoprotein complexes). Moreover, TNPO1 overexpression partially reversed the repressive effect of miR-128 on L1 retrotransposition. Our study represents the first description of a protein factor involved in nuclear import of the L1 element and demonstrates that miR-128 controls L1 activity in somatic cells through two independent mechanisms: direct binding to L1 RNA and regulation of a cellular factor necessary for L1 nuclear import and retrotransposition.

Repetitive elements make up approximately half of the mammalian genomes. A substantial portion of repetitive elements are derived from retrotransposons (LTR-containing and non-LTR), which transpose to new chromosomal locations by reverse transcription of the RNA into DNA, followed by integration of the copied DNA into a new chromosomal location. Retrotransposition of these elements in germ cells leads to integration of new retrotransposons in the genomes of progeny, and because there is no mechanism for excision, they accumulate over evolutionary time scales (1, 2).

Long interspaced element-1 (LINE-1[2] or L1) is the only autonomous transposable element that is currently active in humans and has directly or indirectly contributed to ~ 17% of the human genome (1). Intact, active L1 is ~6 kb in length and contain a 5′ UTR, three open reading frames (ORF1, ORF2, and ORF0), and a short 3′ UTR. The 5′ UTR has promoter activity in both the sense and antisense direction (3–6). ORF1 encodes a protein with RNA-binding and nucleic acid chaperone activity, and ORF2 encodes a protein with endonuclease and reverse transcriptase activities (2, 7–9). ORF0, which is transcribed in the antisense direction, encodes a protein with unknown function that enhances L1 activity. L1 mobilizes replicatively from one place in the genome to another by a "copy and paste" mechanism via an RNA intermediate (10, 11). L1–RNP complexes have been described to enter the nucleus during cell division (12, 13). However, recently, L1 retrotransposition has been demonstrated to also take place in non-diving cells such as neurons (14, 15). The mechanism by which L1–RNP complexes access the host DNA independently of cell division is unknown.

Integration of retrotransposons at new chromosomal locations can generate new genes and affect the expression of already existing genes (16–19). It has been suggested that retrotransposon activity could contribute to various diseases, such as neurological disorders and cancer, as well as developmental defects (20–23). As a result, multiple mechanisms have evolved to tightly control retrotransposon activity. In germ cells, specific small RNA subtypes (piRNAs) efficiently counteract L1 activity (24, 25). In somatic cells, L1 mobilization is potently inhibited by DNA methylation of the L1 promoter (26, 27). However, L1 promoter silencing is greatly attenuated and L1 transcription derepressed in somatic cells under conditions of hypomethylation, often encountered in cancer cells or in *in vitro* reprogramming of somatic cells into induced pluripo-

This work was supported by University of California Cancer Research Coordinating Committee 55205 (to I. M. P.), American Cancer Society Institutional Research Grant 98-279-08 (to I. M. P.), a University of California Irvine Institute for Memory Impairments and Neurological Disorders grant (to I. M. P.), and California Institute of Regenerative Medicine Grant TG2-01152 (to A. I.). The authors declare that they have no conflicts of interest with the contents of this article.

This article contains supplemental Figs. S1–S6.

[1] To whom correspondence should be addressed: University of California, Irvine, Dept. of Molecular Biology and Biochemistry, 3244 McGaugh Hall, 503 Physical Sciences Rd., Irvine, CA 92697-3900. Tel.: (949-824-2587; E-mail: imp@uci.edu.

[2] The abbreviations used are: LINE, long interspaced nuclear element; RNP, ribonucleoprotein; piRNA, Piwi-interacting RNA; iPSC, induced pluripotent stem cell; miRNA, microRNA, miR, microRNA; NLS, nuclear localization sequence; neo, neomycin; RT, reverse transcriptase; RT-qPCR, quantitative real-time PCR; IP, immunoprecipitation.

tent stem cells (iPSCs) (26, 28, 29). Under these conditions, other mechanisms of L1 restriction are important, including DNA, RNA editing proteins, and the microprocessor (AID, APOBECs, ADAR, and DGCR8) (30–33).

The recent discovery of microRNAs (miRNAs or miRs) has revolutionized our understanding of gene control. miRs exemplify the emerging view that non-coding RNAs may rival proteins in regulatory importance. The majority of the human transcriptome is believed to be under miR regulation, positioning this posttranscriptional control mechanism to regulate many gene pathways (32, 34). miRs function as 21- to 24-nt guides that regulate the expression of mRNAs containing complementary sequences. The mature miR is loaded onto specific Argonaute (Ago) proteins, which are then referred to as a miR-inducing silencing complex (34). In animals, partial pairing between a miR and an mRNA target site usually results in reduced protein expression through a variety of mechanisms that involve mRNA degradation and translational repression (35, 36). The best-characterized feature determining miR target recognition are six nucleotide "seed" sites in the 3′ UTR of mRNA targets, which perfectly complement the 5′ end of the miR (positions 2–7) (35).

We recently discovered that miR-128 represses the activity of L1 retrotransposons in somatic cells, analogous to the role of piRNAs in germ cells. We found a novel mechanism for this regulation in that miR-128 binds directly to L1 RNA in the ORF2 coding region sequence, resulting in L1 repression (37). In contrast, miRs typically are thought to repress multiple cellular mRNAs by binding to homologous target sequences; the proteins of these target mRNAs often work in concert, so miRs can fine-tune specific cellular networks (38–41).

In this study, we explored whether miR-128 also regulates L1 activity in somatic cells by repressing cellular proteins important for its retrotransposition. Here we report that miR-128 significantly represses retrotransposition by targeting the nuclear import factor Transportin-1 (TNPO1). TNPO1, also referred to as Karyopherin-β2 or Importin-β2, acts by binding to diverse nuclear localization sequences, including PY-NLSs (37–39). TNPO1-mediated nuclear import requires RanGTP for cargo delivery into the nucleus (42), and known TNPO1 cargoes include viral, ribosomal, and histone proteins (42, 43).

We have determined that miR-128 targets the TNPO1 3′ UTR and represses the expression of TNPO1 mRNA and protein. In addition, we find that TNPO1 facilitates L1 mobilization and that miR-128-induced TNPO1 deficiency represses L1 retrotransposition by inhibiting nuclear import of L1–RNP (using ORF1p as a proxy for L1–RNP complexes). This represents the first description of a cellular host factor likely to be involved in nuclear import of L1. Thus, in summary, we have discovered a dual mechanism by which miR-128 controls L1 mobilization in somatic cells.

Results

miR-128 represses L1 activity

We recently determined that miR-128 directly targets L1 RNA and represses *de novo* retrotransposition and integration in somatic cells, including cancer cells, cancer-initiating cells, and iPSCs, which are all characterized by global demethylation and enhanced opportunity for L1 derepression (37). After demonstrating an important role for miR-128 in the control of L1 retrotransposition in a panel of different cell lines and in iPSCs, we wished to further characterize the mechanism(s) of miR-128-induced restriction of L1 mobilization.

First we initiated analyses to dissect the direct (L1 RNA) *versus* potential indirect (cellular factors) effects of miR-128 on L1 retrotransposition. We performed colony formation assays using different variants of a neomycin reporter constructs encoding the full-length L1 mRNA and a retrotransposition indicator cassette. Briefly, one construct consists of a neomycin gene in the antisense orientation relative to a full-length L1 element, which is disrupted by an intron in the sense orientation (supplemental Fig. S1*A*). The neomycin (neo) protein can be translated into a functional enzyme only after L1 transcription and splicing of the mRNA and reverse transcription followed by integration of the spliced variant into the genome, thus allowing the quantification of cells with new retrotransposition events in culture. In addition, we generated a miR-128–resistant variant of the L1 plasmid by introducing a silent mutation in the miR-128–binding site (in the ORF2 sequence) attenuating miR-128 binding but allowing L1 to retrotranspose (as described in Ref. 37; supplemental Fig. S1*B*). A third variant of the L1 plasmid described in Ref. 44 encodes an L1 RNA harboring a D702A mutation in the RT domain of the ORF2 protein, rendering the encoded L1 RT-deficient (RT-dead). This plasmid variant was used as a negative control (supplemental Fig. S1*C*).

miR-128, anti-miR-128, or miR control shRNAs were cloned into the pMIR-ZIP plasmid and packaged into high-titer lentiviruses, HeLa cells were transduced and puromycin-selected, and modulation of miR-128 expression levels was verified by miR-specific qRT-PCR (supplemental Fig. S2*A*). miR-expressing HeLa cell lines were transfected with either the WT, the miR-128-resistant L1 (mutant), or the RT-deficient L1 (RT-dead) neomycin reporter and selected for 14 days with neomycin replenished daily. We verified that the L1 plasmid was introduced into miR-expressing HeLa cells at equal levels by quantifying the levels of a neomycin-expressing construct (supplemental Fig. S2*B*). We then compared the effect of miR-128 and anti-miR-128 on L1 mobilization with a panel of miR controls (miR-control (miR-control 1), anti-miR-control (miR-control 2), and miR-127, which does not affect L1 retrotransposition (miR-control 3)). In agreement with our previous findings, we observed a significant decrease in the number of neomycin-resistant colonies in cells overexpressing miR-128 and, conversely, a significant increase in neomycin-resistant colonies in anti-miR-128–overexpressing cells (in which endogenously expressed miR-128 is neutralized) relative to HeLa cells with endogenous miR-128 levels, indicating lower *versus* higher rates of active retrotransposition of WT L1, in cells where miR-128 is either overexpressed or neutralized (Fig. 1*A*, *left panel*) (32). Next, analysis of miR-128 regulation of miR-128-resistant L1 retrotransposition (mutant) was performed to evaluate potential indirect regulation of L1 by miR-128. We found that miR-128 induction significantly repressed mobilization of miR-128–resistant L1 and that miR-128 neu-

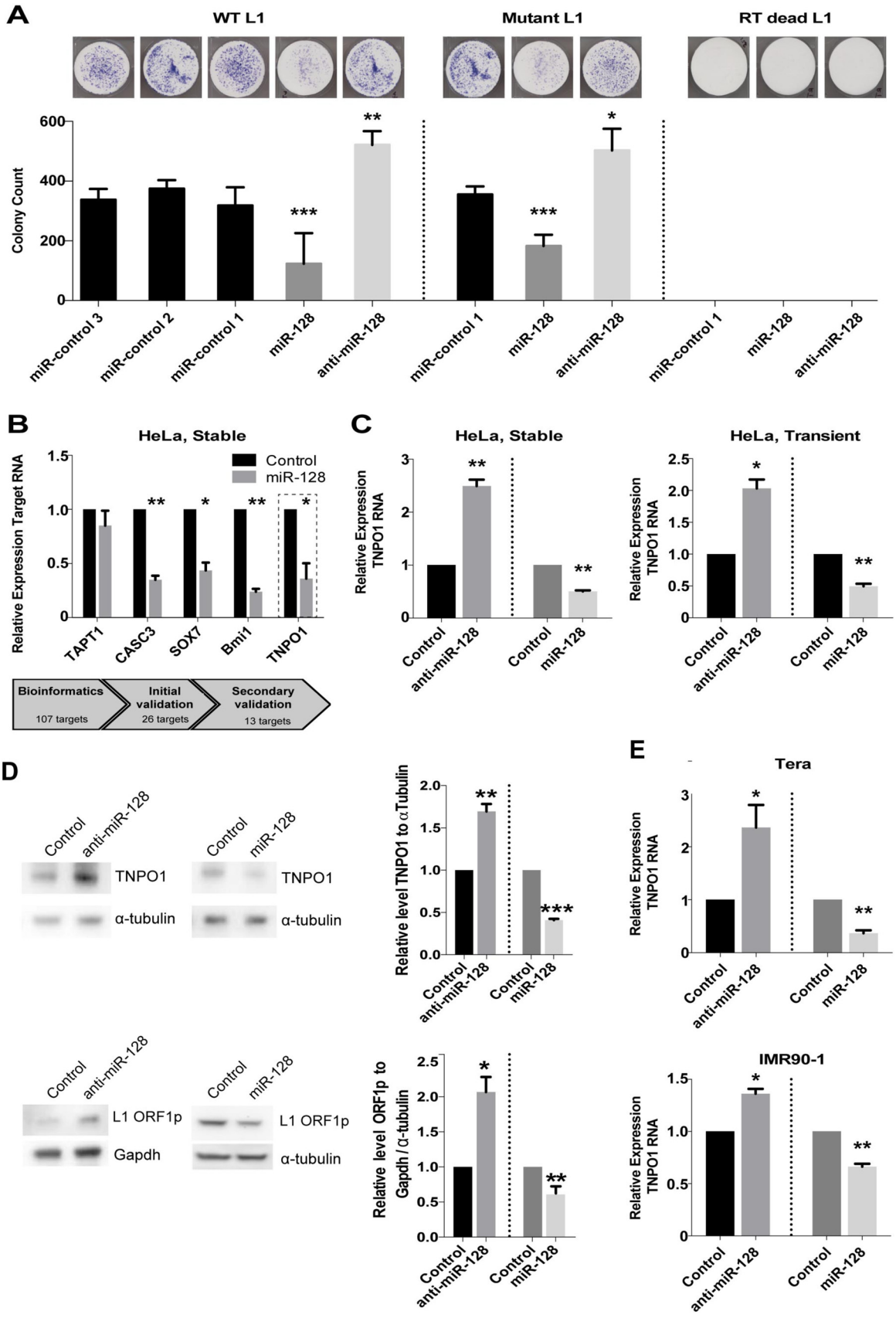
A
WT L1
Mutant L1
RT dead L1
Colony Count
600
400
200
0
**
***
*
***
*
miR-control 3
miR-control 2
miR-control 1
miR-128
anti-miR-128
miR-control 1
miR-128
anti-miR-128
miR-control 1
miR-128
anti-miR-128
B
HeLa, Stable
Relative Expression Target RNA
Control
miR-128
1.5
1.0
0.5
0
TAPT1
CASC3
SOX7
Bmi1
TNPO1
Bioinformatics
107 targets
Initial validation
26 targets
Secondary validation
13 targets
C
HeLa, Stable
Relative Expression TNPO1 RNA
Control
anti-miR-128
Control
miR-128
HeLa, Transient
Relative Expression TNPO1 RNA
Control
anti-miR-128
Control
miR-128
D
Control
anti-miR-128
Control
miR-128
TNPO1
α-tubulin
TNPO1
α-tubulin
Relative level TNPO1 to αTubulin
Control
anti-miR-128
Control
miR-128
L1 ORF1p
Gapdh
L1 ORF1p
α-tubulin
Relative level ORF1p to Gapdh / α-tubulin
Control
anti-miR-128
Control
miR-128
E
Tera
Relative Expression TNPO1 RNA
Control
anti-miR-128
Control
miR-128
IMR90-1
Relative Expression TNPO1 RNA
Control
anti-miR-128
Control
miR-128

tralization by anti-miR-128 significantly enhanced mobilization of miR-128–resistant L1 relative to miR control (Fig. 1*A*, *center panel*). Importantly, miR-modulated HeLa cells encoding RT-deficient L1 (RT-dead) resulted in no neomycin-resistant colonies, demonstrating that colonies obtained upon wild-type and miR-128–resistant L1 plasmid transfections and neo selection are the consequence of a round of *de novo* L1 (Fig. 1*A*, *right panel*) (44, 45). These results support the idea that miR-128 functions through direct binding of L1 RNA and by regulating cellular co-factors on which L1 is dependent for successful mobilization.

Identification of miR-128 targets involved in regulation of L1 retrotransposition

miRs often exert their regulatory roles of complex cellular functions by repressing multiple targets in the same signaling pathway. Therefore, miRs can be thought of as master RNA regulators, similar to transcription factors, which are DNA regulators. We have employed different strategies to identify miR-128 targets that may work in synergy with direct L1 RNA targeting to limit L1 mobilization. We performed an unbiased screen to validate bioinformatically predicted miR-128 targets by using PicTar and TargetScan (46, 47) (Fig. 1*B*, *top panel*). HeLa cells were transfected with miR-128 or control miR mimics, 107 targets were analyzed by qRT-PCR, and 13 potential miR-128 targets were verified twice, including TAPT1, CASC3, SOX7, BMI-1, and TNPO1 (Fig. 1*B*, *bottom panel*, and supplemental Fig. S3).

An area of L1 biology the literature is conflicted about deals with whether L1–RNP complexes are dependent on cell division for nuclear import (12, 13, 15). Interestingly, Macia *et al.* (15) recently demonstrated that L1 can retrotranspose efficiently in mature nondividing neuronal cells; however, the mechanism responsible for active nuclear import is unknown. With this in mind, we were excited to identify TNPO1 as a potential miR-128 target, as TNPO1 functions in nuclear import of a variety of RNA-binding proteins critical for various steps in gene expression (48, 49).

We determined that stably transduced HeLa cells expressing anti-miR-128 exhibit significantly higher levels of TNPO1 mRNA relative to the control sequence (Fig. 1*C*, *left panel*), in contrast to miR-128–overexpressing HeLa cells, in which TNPO1 mRNA was significantly reduced (Fig. 1*C*, *left panel*). To rule out the possibility that the observed miR-128 effect was an artifact stemming from genomic integration of lentiviral encoded miRs, we transiently transfected miR-128, anti-miR-128, or control miR mimic oligonucleotides into HeLa cells as an alternative approach and verified the effect of miR-128 and anti-miR-128 relative to miR controls (Fig. 1, *C*, *right panel*, and *B*, *bottom panel*). Next, we determined that miR-128 *versus* anti-miR-128 regulated the protein level of TNPO1, correlating with the observed changes in expression levels of TNPO1 mRNA (Fig. 1*D*, *top panel*; quantifications, *top right panel*) and that these changes were accompanied by significant ORF1p reductions *versus* increases (Fig. 1*D*, *bottom panel*; quantification, *bottom right panel* and Ref. 37). Finally, to exclude the possibility that miR-128 exclusively targets TNPO1 mRNA in HeLa cells, we tested a teratoma cell line (Tera-1) and an iPSC line (IMR90). We found that TNPO1 mRNA expression levels were significantly changed in Tera-1 and IMR90 cells in addition to HeLa cells (Fig. 1, *C* and *E*). These combined results show that miR-128 regulates the expression levels of TNPO1 in different cell types.

miR-128 interacts with a target sequence in the 3′ UTR of TNPO1 mRNA

Next we wished to examine whether miR-128 indirectly regulates TNPO1 expression or directly interacts with TNPO1 mRNA. Bioinformatics analyses identified three potential seed matches in TNPO1 mRNA (Fig. 2*A*). The TNPO1 3′ UTR and coding reading frame sequence, including the three potential miR-128–binding sites, were cloned into a luciferase-based miR-binding site reporter construct. In addition, a perfect 23-nt miR-128 sequence (positive control) luciferase construct was generated. HeLa cells were transfected with one of the TNPO1 binding site–encoding plasmids in addition to mature miR-128 or miR control mimics. Luciferase activity was significantly reduced in cells transfected with miR-128 and encoding binding site 1 (8-mer perfect seed site in the 3′ UTR) (Fig. 2, *A* and *B*). In contrast, miR-128 expression did not substantially reduce luciferase activity in cells encoding binding site 2 or 3. These results indicate that miR-128 preferentially targets TNPO1 mRNA by binding to site 1.

Next, mutations were introduced into the putative miR-128–binding site in the TNPO1 mRNA encoding site 1 in the 3′ UTR (Fig. 2*A*) to determine whether this sequence is responsible for the interaction with miR-128 (Fig. 2*C*, *top panel*). The luciferase activity was again significantly lower than that of con-

Figure 1. Identification and verification of TNPO1 as a cellular target of miR-128. *A*, change in colony count of neomycin-resistant foci was used to determine the level of active retrotransposition in HeLa cells stably transduced with lentiviral constructs encoding a control miRs (*control 1*, *2*, and *3*), anti-miR-128, or miR-128 transfected with the L1 expression plasmid (wild-type L1, *left panel*). Colony formation assays were performed as described above using a miR-128–resistant L1 expression plasmid (*Mutant*) or reverse transcriptase–incompetent L1 expression plasmid (*RT dead L1*). Data are shown as mean ± S.E. ($n = 3$ independent biological replicates; *, $p < 0.05$; **, $p < 0.01$; ***, $p < 0.001$). *B*, schematic of the miR-128 qPCR screen approach. HeLa cells were transiently transfected with miR-128 or control miR mimic, cells were harvested after 72 h, RNA was isolated, and qPCR was performed for predicted miR-128 targets using GAPDH as a housekeeping gene (*bottom panel*). Thirteen targets were validated as down-regulated in miR-128–treated cells (supplemental Fig. 3), and relative levels of five targets, TAPT1, CASC3, SOX7, Bmi1, and TNPO1 RNA, normalized to B2M are shown as mean ± S.E. ($n = 3$ independent biological replicates; *, $p < 0.05$; **, $p < 0.01$) (*top panel*). *C*, relative levels of TNPO1 RNA normalized to B2M in HeLa cells stably transduced or transiently transfected with control miR, anti-miR-128, or miR-128 are shown as mean ± S.E. ($n = 3$ independent biological replicates; *, $p < 0.05$; **, $p < 0.01$). *D*, HeLa cells were stably transduced with control, anti-miR-128, or miR-128 lentiviral constructs, and Western blot analyses were performed for TNPO1 (*top left panel*), L1 ORF1p (*bottom left panel*), α-tubulin, or GAPDH protein. One representative example of three is shown. Quantification of results ($n = 3$) normalized to tubulin (TNPO1) or GAPDH (L1 ORF1p) are shown (*right panels*). *E*, relative levels of TNPO1 RNA normalized to B2M were determined in a teratoma cell line (*Tera*) stably transduced with control miR, anti-miR-128, or miR-128 and iPSCs (*IMR90-1*) transiently transfected with control miR, anti-miR-128, or miR-128 mimics ($n = 3$ independent biological replicates; *, $p < 0.05$; **, $p < 0.01$). Throughout the figure, *, $p < 0.05$; **, $p < 0.01$ by two-tailed Student's *t* test. Uncropped versions of blots are shown in supplemental Fig. 5.

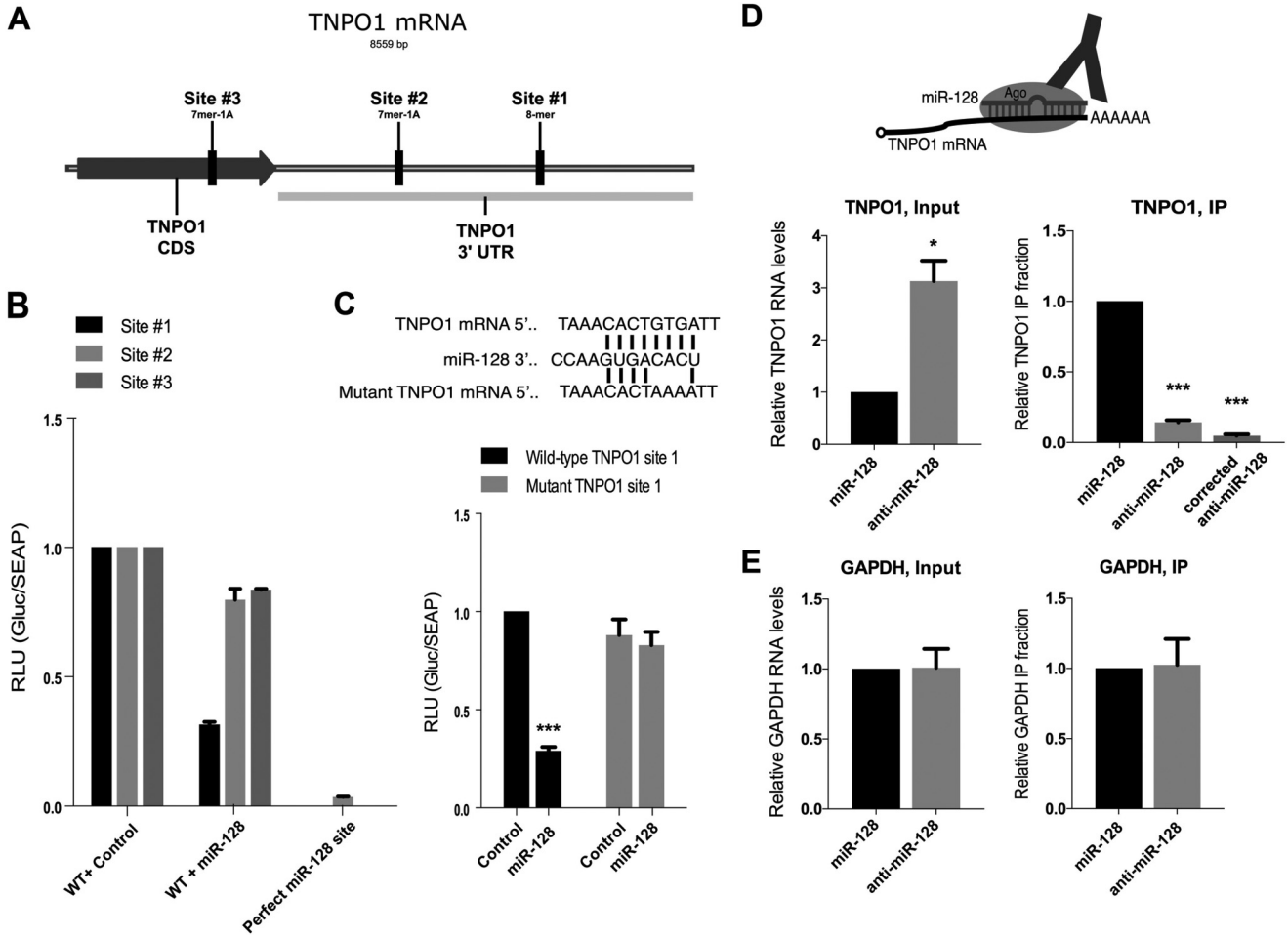

Figure 2. miR-128 represses TNPO1 by binding directly to the 3′ UTR of TNPO1 mRNA. *A*, schematic of the three predicted miR-128 binding sites in the TNPO1 mRNA (coding DNA sequence (*CDS*) and 3′ UTR are shown). miR-128 binding site 1 in the TNPO1 3′ UTR is a perfect 8-mer seed site; site 2 (in the 3′ UTR) and site 3 (in the coding region sequence) are both 7-mer seed binding sites. *B*, relative luciferase levels of HeLa cells transfected with constructs expressing a luciferase gene fused to the WT binding sequence for sites 1, 2, or 3 or the positive control sequence corresponding to the 22-nt perfect match of miR-128 along with transfections of control or miR-128 mimics were determined 48 h post-transfection. Results are shown as mean ± S.E. ($n = 3$ independent biological replicates. *C*, schematic of miR-128 binding to WT TNPO1 3′ UTR mRNA or mutant seed site TNPO1 mRNA (*top panel*). Relative luciferase levels of HeLa cells transfected with the reporter plasmid for WT site 1 or mutated site 1 co-transfected with control miR or miR-128 mimics were determined 48 h post-transfection. Results are shown as mean ± S.E. ($n = 3$ independent biological replicates; ***, $p < 0.001$). *D*, schematic of the Ago immunopurification strategy of miR-128-TNPO1 mRNA complexes (Ago-RIP) (*top panel*). HeLa cell lines are generated where miR-128 is either stably neutralized (by anti-miR-128) or overexpressed. Relative expression of TNPO1 mRNA normalized to B2M is shown for input samples (*bottom left panel*); relative fraction of TNPO1 transcript levels associated with Ago complexes is shown for IP samples (*bottom right panel*). TNPO1 IP fractions normalized to the levels of TNPO1 in input are shown as "corrected" (*bottom right panel*). Results shown as mean ± S.E. ($n = 3$ independent biological replicates; *, $p < 0.05$; ***, $p < 0.001$). *E*, relative levels of GAPDH in the same input and IP samples were determined as a negative control. Results are shown as mean ± S.E. ($n = 3$ independent biological replicates).

trols in HeLa cells transfected with the WT TNPO1 site 1 plasmid and mature miR-128, supporting the conclusion that miR-128 can bind to the WT TNPO1 3′ UTR sequence and prevented the translation of luciferase (Fig. 2*C*, *bottom panel*). In contrast, HeLa cells transfected with the mutant TNPO1 3′ UTR mutant–binding site and mature miR-128 or control miRs exhibited luciferase activity at the same levels as the WT TNPO1 and miR-control cells, consistent with the conclusion that miR-128 could no longer bind and repress reporter gene expression (Fig. 2*C*, *bottom panel*).

Furthermore, Ago complexes containing miRs and target mRNAs were isolated by immunopurification and assessed for relative complex occupancy by the TNPO1 mRNA to validate that miR-128 directly targets TNPO1 mRNA in cells (Fig. 2*D*, *top panel*) in miR-128– *versus* anti-miR-128–overexpressing HeLa cells, as described previously (37). The relative level of TNPO1 mRNA was significantly lower in cells stably overexpressing miR-128 compared with those expressing anti-miR-128 constructs, as expected (Fig. 2*D*, *bottom left panel*, *Input*). Despite the increased levels of TNPO1 mRNA (because of lower miR-128 expression levels), which may underestimate the scale of the effect, the relative fraction of Ago-bound TNPO1 mRNA significantly increased when miR-128 was overexpressed (Fig. 2*D*, *bottom right panel*, *IP*). When correcting for the lower expression level of TNPO1 mRNA, the increase in miR-128–bound TNPO1 mRNA was even more significant (Fig. 2*D*, *top panel*). In contrast, miR-128 did not repress GAPDH mRNA expression levels or immunopurified gapdh mRNA, as expected (Fig. 2*E*). We interpret this to mean that high levels of miR-128 lead to higher levels of TNPO1 mRNA being bound and regulated directly by miR-128. These data support the conclusion that miR-128 represses TNPO1

expression via a direct interaction with the target site located in the 3′ UTR of the TNPO1 mRNA.

TNPO1 modulation regulates L1 activity and de novo retrotransposition

TNPO1 functions by interacting with nuclear localization sequences on protein cargoes and facilitates nuclear import (48, 50–52). We hypothesized that L1–RNP may utilize TNPO1-dependent active transport in addition to accessing the host DNA during cell division.

First we wished to evaluate whether TNPO1 directly plays a role in L1 mobilization. For this purpose, we generated TNPO1 constructs expressing TNPO1 shRNA (to obtain TNPO1 knockdown HeLa cells) or encoding the full-length TNPO1 mRNA transcript harboring the 5.6-kb 3′ UTR, including the miR-128–binding site (to generate HeLa cells overexpressing TNPO1) and control plasmids. We verified that TNPO1 shRNA or overexpression plasmids significantly reduced *versus* increased mRNA of TNPO1 relative to controls (Fig. 3*A*). We also evaluated whether TNPO1 knockdown or overexpression are toxic to cells or affect cell proliferation. Morphological and cell proliferation analysis of TNPO1-modulated HeLa cells showed that TNPO1 knockdown or overexpression is not toxic to HeLa cells, which proliferate at a similar rate relative to plasmid control HeLa cells (supplemental Fig. S4*A*). Because HeLa cells express low levels of endogenous L1 activity, we transiently transfected a construct encoding the full-length WT L1 and monitored the effects of TNPO1 depletion on artificially expressed L1 mRNA. We then performed colony formation assays to determine a possible requirement of TNPO1 in new L1 retrotransposition events. We verified that the L1 plasmid was introduced into TNPO1-expressing HeLa cells at similar levels by quantifying the levels of the neo-encoding expression plasmid (supplemental Fig. S2, *C* and *D*). We then determined that cells deficient in TNPO1 exhibited a significantly lower number of neomycin-resistant colonies *versus* cells overexpressing TNPO1, which showed a significant increase in neomycin-resistant colonies relative to controls (Fig. 3*B*). This is consistent with lower *versus* higher rates of *de novo* retrotransposition and genomic integration (Fig. 3*B*, shown as colony counts (percent) and colony counts). TNPO1-modulated HeLa cells encoding RT-deficient L1 (RT-dead) resulted in no neomycin-resistant colonies, demonstrating that colonies obtained upon wild-type L1 plasmid transfections and neo selection are the consequence of a round of *de novo* L1 (data not shown). Next, protein lysates from TNPO1-deficient cells and TNPO1-overexpressing cells were prepared, and TNPO1 and ORF1p protein levels were found to be significantly reduced in TNPO1-deficient cells and increased in TNPO1-induced cells compared with controls (Fig. 3*C*, *top panels*; quantification, *bottom panels*). The amount of L1 mRNA (ORF2) was regulated by TNPO1, consistent with the observed effect on L1 protein (ORF1p) abundance (data not shown). We noticed that the global amount of L1 protein changes when TNPO1 levels change. This may be a consequence of accelerated degradation of L1-RNP components caused by dysregulated nuclear transport of L1. These combined data support the conclusion that TNPO1 neutralization or overexpression results in a corresponding decrease or increase in new retrotransposition events and establish a role of TNPO1 as a novel and specific modulator of L1 activity.

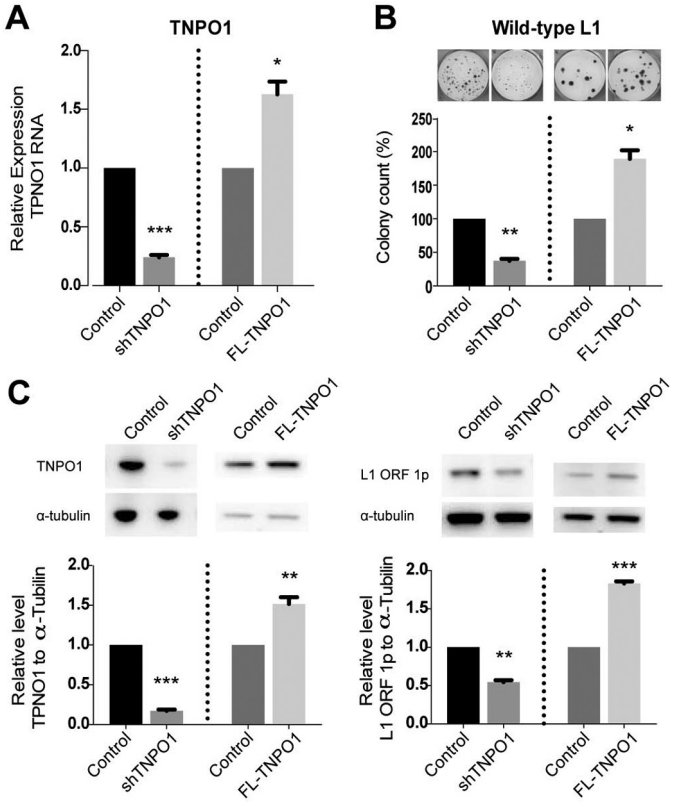

Figure 3. TNPO1 knockdown reduces L1 activity, whereas TNPO1 overexpression enhances L1 retrotransposition. *A*, relative expression of TNPO1 RNA normalized to B2M in the same samples was determined (*right*). Results shown as a mean ± S.E. ($n = 3$ independent biological replicates; *, $p < 0.05$; ***, $p < 0.001$). *B*, *de novo* retrotransposition was determined by quantification of neomycin-resistant foci of HeLa cells stably transfected with plasmids encoding controls (*Control*), shTNPO1, FL-Control, or FL-TNPO1 co-transfected with the L1 expression plasmid (*Wild-type L1*). Data are shown as mean ± S.E. ($n = 3$ independent biological replicates; *, $p < 0.05$; **, $p < 0.01$). *C*, relative expression of amount of ORF2 normalized to B2M in HeLa cells stably transfected with a shControl (*Control*), shTNPO1, FL-Control (*Control*), or full-length TNPO1 overexpression (*FL-TNPO1*) plasmid (*left*). *D*, Western blot analysis of TNPO1 and α-tubulin (protein levels in HeLa cells stably transduced with controls, shTNPO1, or FL-TNPO1 plasmid) (*left*). One of three representative examples is shown. Quantification of results ($n = 3$) normalized to α-tubulin is shown (*right*). Uncropped versions of blots are shown in supplemental Fig. 5.

TNPO1 depletion inhibits L1 nuclear import

TNPO1 belongs to the family of transportins, which also includes TNPO2 and TNPO3 (49). All three protein subtypes are expressed in all examined tissues and function in nuclear import (48–52). Reminiscent of the generally accepted role TNPO3 plays in nuclear import of the preintegration complex of HIV-1 (6, 53–59), we next decided to explore whether TNPO1 functions in a similar manner by assisting with the nuclear import of the L1–RNP complex. Faced with the difficulties of investigating RNA and proteins encoded by endogenous L1s, we developed a construct expressing a tagged protein of L1 containing HA (ORF1p-HA) and used localization of ORF1p as a proxy to reflect localization of L1–RNP, keeping in mind the limitations of this approach. We generated stable

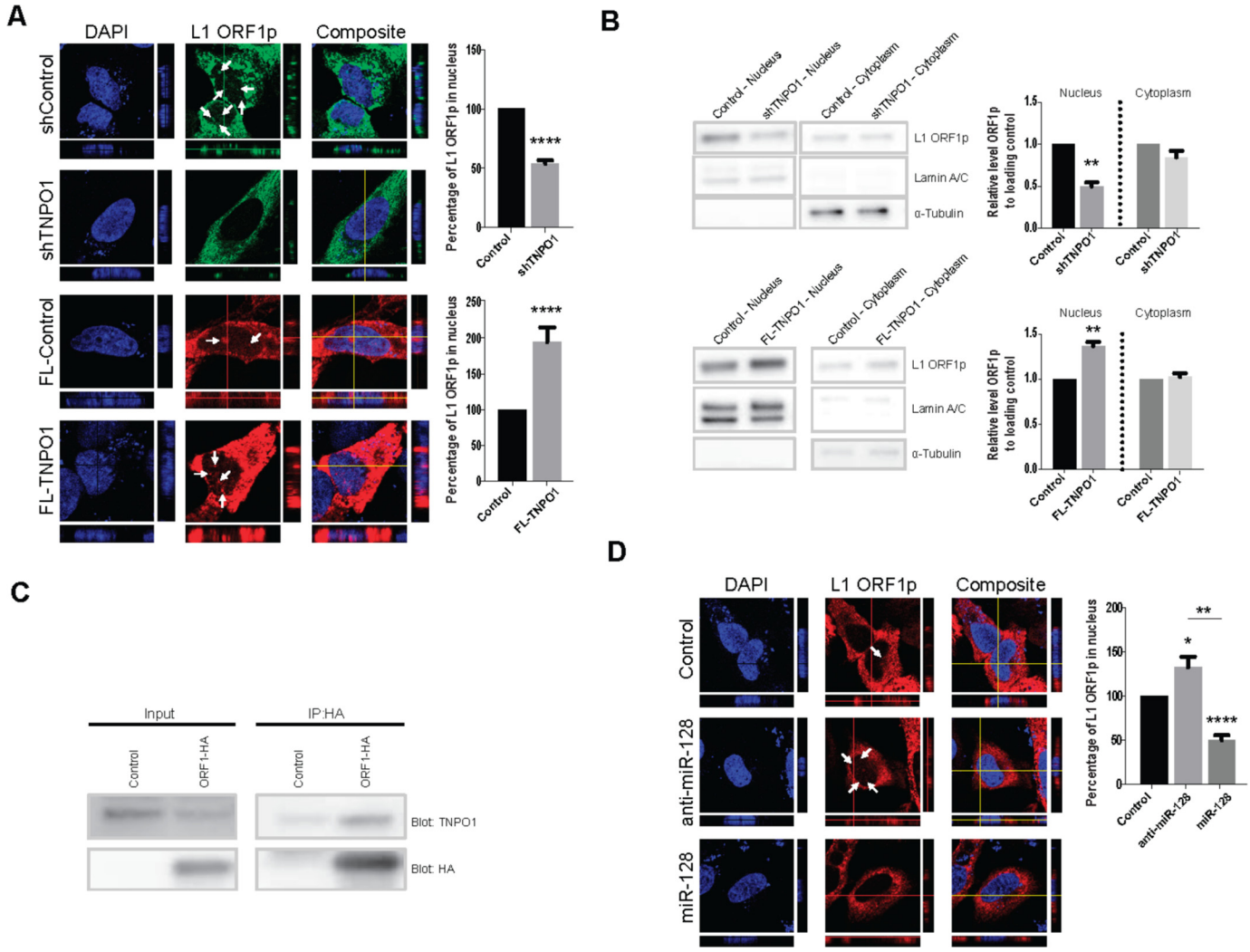

Figure 4. TNPO1 knockdown reduces nuclear import of L1 (ORF1p), whereas induced expression of TNPO1 enhances nuclear import of L1 (ORF1p). *A*, localization of L1 ORF1p-HA was determined in HeLa cells stably expressing controls, shTNPO1, or FL-TNPO1 and then co-transfected with full-length WT L1 and ORF1p-HA or control vector. Representative orthogonal views of z-stack images are shown. Quantification of L1 ORF1p-HA localization to the nucleus is shown (represented as a percentage of L1 ORF1p in the nucleus/all L1 ORF1p in the image; *arrows* indicate examples of ORF1p nuclear staining in the single-channel images). Results are shown as the mean percentage of L1 ORF1p in the nucleus ± S.E. ($n = 50$ technical replicates of 3 independent biological replicates; ****, $p < 0.0001$). TAF15, a verified TNPO1 cargo, was used as a positive control (supplemental Fig. 4*D*). *B*, subcellular fractionation analysis was performed on TNPO1-modulated HeLa cells that were co-transfected with full-length WT L1 and ORF1p-HA or control vector. Western blot analysis of L1-ORF1p-HA, Lamin A/C, or α-tubulin protein levels in nuclear (*N*) or cytoplasmic (*C*) fractions of HeLa cell protein-containing lysates stably expressing controls, shTNPO1 or FL-TNPO1 (one representative of three) is shown. Quantification of results ($n = 3$) normalized to Lamin A/C (nuclear), or α-tubulin (cytoplasmic) is shown. **, $p < 0.01$. *C*, HeLa cells were transfected with ORF1-HA expression plasmid, HA was immunoprecipitated, and co-immunoprecipitated TNPO1 was determined by blotting for native TNPO1. One representative example of two is shown. *D*, localization of L1 ORF1p-HA was determined in HeLa cells stably transduced with miR control (*control*), anti-miR-128, or miR-128 and then transfected with the ORF1p-HA expression plasmid. Representative orthogonal views of z-stack images are shown. Quantification of L1 ORF1p-HA localization to the nucleus (represented as a percentage of L1 ORF1p in the nucleus/all L1 ORF1p in the image; *arrows* indicate examples of ORF1p nuclear staining) is shown as the mean percentage of L1 ORF1p in the nucleus ± S.E. ($n = 50$ technical replicates of 3 independent biological replicates; *, $p < 0.05$; **, $p < 0.01$; ****, $p < 0.0001$). Uncropped versions of the blots are shown in supplemental Fig. 5.

TNPO1-overexpressing and TNPO1 knockdown HeLa cell lines that were transiently co-transfected with full-length WT L1 and ORF1p-HA or control vector, and ORF1p localization was visualized and quantified by immunofluorescence confocal analysis. As the FL-TNPO1 plasmid co-expresses GFP, an alternate secondary antibody was used to visualize ORF1p in TNPO1-induced HeLa cell lines (Alexa Fluor 568). We determined that TNPO1 reduction (shTNPO1) resulted a significant reduction of nuclear ORF1p (as determined by ORF1p expression in the nucleus as a measure of total cellular ORF1p) (Fig. 4*A*, *top panels*; quantification, *top right panel*; *arrows* indicate examples of ORF1p nuclear staining in the single-channel images), and overexpression of TNPO1 (FL-TNPO1) resulted in a significant increase in the localization of ORF1p in the nucleus compared with control cells (Fig. 4*A*, *bottom panels*; quantification, *bottom right panel*). Untransfected cells are shown in supplemental Fig. S4*C*. As a positive control, a known TNPO1 interaction partner, TBP-associated factor 15 (TAF15), was also analyzed (60). As expected, TNPO1 knockdown decreased the nuclear localization of TAF15, which was, instead, found in the cytoplasm and at the plasma membrane (supplemental Fig. S4*D*).

Next we subjected TNPO1-modulated HeLa cell lines that were transiently co-transfected with full-length WT L1 and ORF1p-HA to subcellular fractionation analysis, keeping in mind the limitation of this approach. Nuclear and cytoplasmic fractionations were evaluated by determining the expression levels of α-tubulin (cytoplasmic) and Lamin A/C (nuclear) (Fig. 4*B*, *left panels*), and TNPO1 knockdown and overexpression were verified by qRT-PCR (supplemental Fig. S4*B*). We next examined the effect of TNPO1 modulation on encoded L1 protein (ORF1p) as an indirect measure of L1-RNP localization. Analyzing the ORF1p levels in nuclear *versus* cytoplasmic fractions from TNPO1 knockdown HeLa cells lines (shTNPO1) (shown in Fig. 3*C*, *left panel*) showed a substantial decrease in ORF1p levels in the nucleus relative to controls (Fig. 4*A*, *top panels*). Overexpression of TNPO1 (FL-TNPO1) resulted in increased nuclear L1 ORF1p expression compared with controls (Fig. 4*B*, *bottom panels*). We did not observe a significant change in ORF1p levels in the cytoplasmic fractions. This is not too surprising, as the vast majority of ORF1p is localized in the cytoplasm; thus, changes in expression levels might not be measurable, as opposed to expression levels in the nucleus. We noted that ORF1p levels as determined by Western blot analysis following subcellular fractionation surprisingly showed a ratio of less ORF1p in the cytoplasm *versus* the nucleus. This finding was in contrast to our confocal analysis of ORF1p localization. This difference is possibly due to a much more dilute cytoplasmic fraction compared with nucleic fraction. However, even with these limitations in mind, the combined results from the confocal and subcellular fractionation analysis indicate that TNPO1 is facilitating L1 access to host DNA.

Furthermore, we performed immunoprecipitation analysis to evaluate whether TNPO1 interacts with ORF1p. HeLa cells were transduced with a tagged version of ORF1 (ORF1p-HA), protein-containing lysates were prepared, and ORF1p immunoprecipitations were performed and blotted for TNPO1 and HA. The ORF1p co-immunoprecipitations results suggest that ORF1p (L1–RNP complex) and TNPO1 interact (Fig. 4*C*). However, further studies are needed to determine whether this interaction is direct or indirect through an RNA bridge, as demonstrated previously for many ORF1p binding partners (61).

Finally, we evaluated the effect of miR-128-induced TNPO1 repression on L1 nuclear import. miR-128, anti-miR-128, or control miR HeLa cells were transfected with ORF1p-HA expression plasmids, and localization of L1 was analyzed by confocal analysis, as described above. miR-128–mediated TNPO1 repression (verified and shown in Fig. 1*D*, *top panel*) resulted in a significant decrease in L1 ORF1p nuclear localization (Fig. 4*D*, *left panel*, *right column*; quantification, *right panel*), whereas anti-miR-128-induced TNPO1 expression significantly increased nuclear L1 ORF1p expression levels (Fig. 4*D*, *left panel*, *center column*; *arrows* indicate examples of ORF1p nuclear staining in the single-channel images; quantification, *right panel*).

This body of work supports the idea that miR-128–induced TNPO1 repression results in a modest but significant and reproducible decrease in nuclear import of some L1–RNP complexes or components of L1–RNP complexes (using ORF1p as a proxy), accumulation of L1 (ORF1p) in the cytoplasm, and a significant reduction in L1 retrotransposition events. Additional studies are needed to determine whether functional L1–RNP complexes are actively transported into the nucleus and whether this event is facilitated by TNPO1. In summary, our findings support the idea that, in addition to direct access of L1–RNP to host DNA during cell division, some L1–RNP complexes are imported into the nucleus via TNPO1.

TNPO1 is a functional target of miR-128–induced L1 repression

We have demonstrated previously that miR-128 targets L1 RNA and represses L1 activity by a direct interaction, similar to how miRs represses replication of RNA virus (62, 63). In addition, we have now determined that miR-128 is capable of repressing miR-128–resistant L1 (using a L1 mutant vector) by an indirect mechanism (Fig. 1*A*). With this in mind, we wished to evaluate the significance of TNPO1 as a functional mediator of miR-128–induced L1 repression.

We utilized the L1 mutant vector, in which the miR-128–binding site had been mutated and miR-128 is no longer able to bind (miR-128–resistant L1). In addition, to perform TNPO1 rescue experiments, we needed to overexpress a miR-128–resistant version of the TNPO1 vector, as miR-128 may otherwise be able to bind to the WT TNPO1 plasmid and could, in theory, function as a miR-128 sponge. We generated a miR-128–resistant full-length TNPO1 vector in which miR-128–binding site 1 in the 3′ UTR had been mutated according to our mutation analysis, and miR-128 was no longer able to bind (Fig. 2*C*) (FL-TNPO1mut).

We found that overexpression of TNPO1 (WT and miR-128–resistant) in miR-128–overexpressing HeLa cells were able to partially but significantly rescue miR-128–induced repression of L1 retrotransposition and genomic integration, as determined by colony formation assays, relative to controls for WT L1 (Fig. 5*A*, *left panel*, and supplemental Fig. S6*A*). Similar results were obtained when rescuing miR-128 L1 restriction with TNPO1 (WT and miR-128–resistant) of the Mutant L1 plasmid relative to controls (Fig. 5*A*, *right panel*, and supplemental Fig. S6*A*). Cellular localization of L1 (ORF1p) by confocal analysis suggested that miR-128–induced reduction of nuclear localization of ORF1p was partly but significantly rescued by overexpressing TNPO1 (WT and miR-128–resistant) compared with controls (Fig. 5*B*, *arrows* indicate examples of ORF1p nuclear staining in the single-channel images; quantification, *right panels*; see supplemental Fig. S6*B* for WT L1 confocal images). Finally, we analyzed the amount of ORF2 mRNA as an indirect measure for L1 RNA under the same experimental conditions and found that TNPO1 overexpression rescued the miR-128–induced decrease in ORF2 amount relative to control cells (supplemental Fig. S6*C*). These results show that overexpression of both WT and miR-128–resistant TNPO1 can partly rescue miR-128–induced L1 restriction.

Finally, we performed experiments in which we depleted cells of TNPO1 (using TNPO1 shRNA) in anti-miR-128 stable HeLa cells (in which endogenous levels of miR-128 are neutralized). TNPO1 depletion in anti-miR-128 HeLa cells resulted in

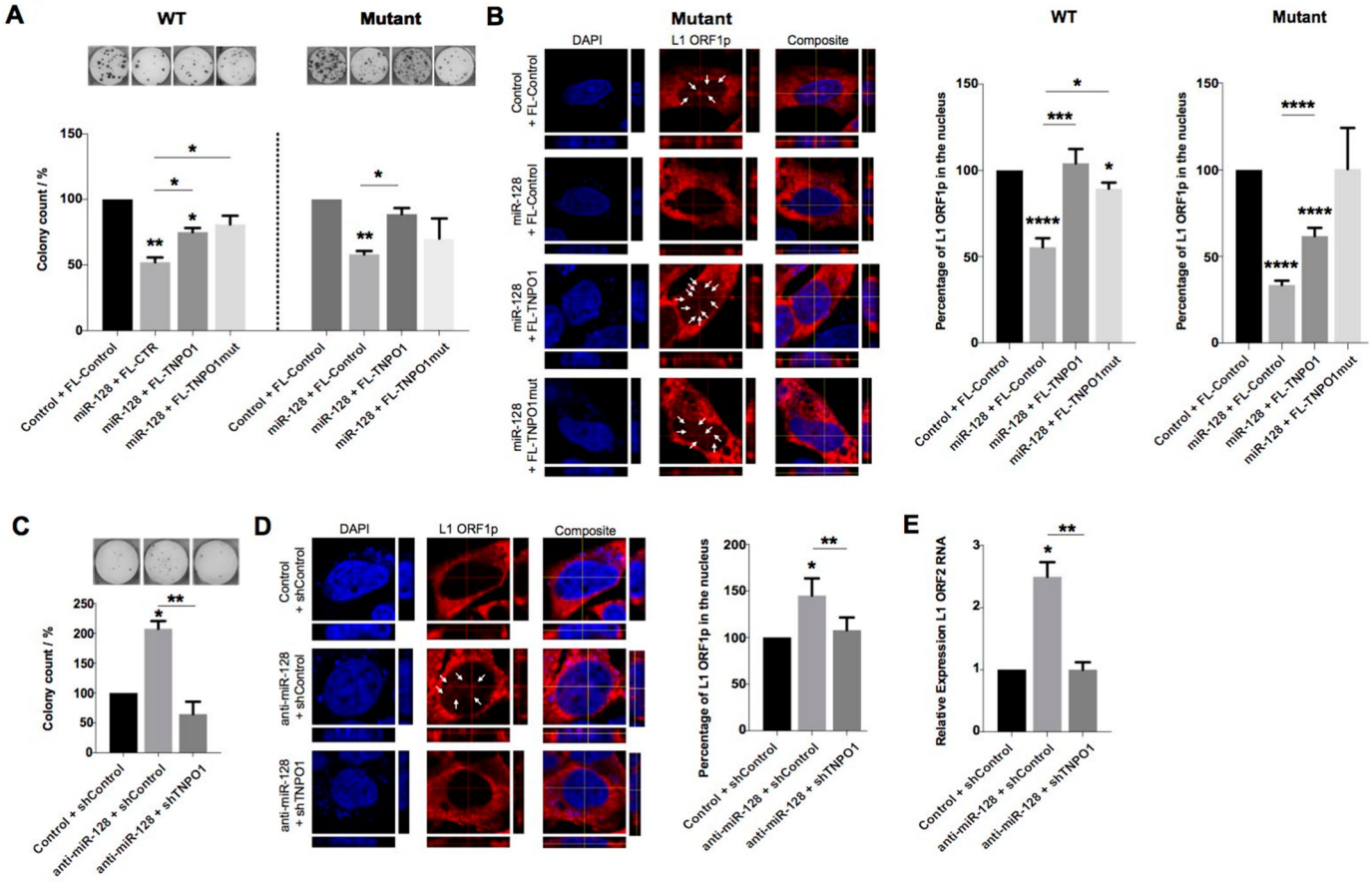

Figure 5. TNPO1 partly rescues miR-128-induced repression of L1 retrotransposition and genomic integration. *A*, *de novo* retrotransposition was determined by the change in colony count of neomycin-resistant foci of HeLa cells stably transduced with control miR (*control*) or miR-128 transfected with FL-control, FL-TNPO1, or FL-TNPO1mut (miR-128–resistant) and co-transfected with the miR-128 mutant L1 expression plasmid. Results are shown as mean ± S.E. ($n = 3$ independent biological replicates; *, $p < 0.05$; **, $p < 0.01$; supplemental Fig. S6*A*). *B*, localization of L1 ORF1p-HA was determined in HeLa cells stably transduced with control miR (*control*) or miR-128, then transfected with FL-control, FL-TNPO1, or FL-TNPO1mut, and co-transfected with the miR-128 mutant L1 expression plasmid. Representative orthogonal views of z-stack images are shown. Quantification of L1 ORF1p-HA localization to the nucleus is shown as the mean percentage of L1 ORF1p in the nucleus (represented as a percentage of L1 ORF1p in the nucleus/all L1 ORF1p in the image; *arrows* indicate examples of ORF1p nuclear staining in the single-channel images) ± S.E. ($n = 50$ technical replicates of 3 independent biological replicates; *, $p < 0.5$; ***, $p < 0.001$; ****, $p < 0.0001$; supplemental Fig. S6*B*). *C*, new retrotransposition events were determined by change in colony count of neomycin-resistant foci in HeLa cells stably transduced with control miR (*control*) or anti-miR-128 transfected with shControl or shTNPO1 and co-transfected with the WT L1 expression plasmid. Results are shown as mean ± S.E. ($n = 3$ independent biological replicates; *, $p < 0.05$; **, $p < 0.01$). *D*, localization of L1 ORF1p-HA was determined in HeLa cells stably transduced with control miR (*control*) or anti-miR-128, then transfected with shControl or shTNPO1, and co-transfected with the WT L1 expression plasmid. Representative orthogonal views of z-stack images are shown. Quantification of L1 ORF1p-HA localization to the nucleus is shown as the mean percentage of L1 ORF1p in the nucleus (*arrows* indicate examples of ORF1p nuclear staining in the single-channel images) ± S.E. ($n = 50$ technical replicates of 3 independent biological replicates; *, $p < 0.05$; **, $p < 0.01$). *E*, relative expression of the ORF2 amount normalized to B2M in HeLa cells stably transduced with control miR (*control*) or anti-miR-128, transfected with shControl or shTNPO1, and co-transfected with the wild-type L1 plasmid. Results are shown as mean ± S.E. ($n = 3$ independent biological replicates; *, $p < 0.05$; **, $p < 0.01$).

a partial and significant rescue of the inhibitory effect of miR-128 on L1 retrotransposition and integration relative to control, as determined by colony formation assays (Fig. 5*C*), L1 ORF1p nuclear localization by confocal analysis (Fig. 5*D*, *arrows* indicate examples of ORF1p nuclear staining in the single-channel images; quantification, *right panel*), and amount of ORF2 mRNA (Fig. 5*E*). These combined results strongly support the idea that TNPO1 is a functional target for miR-128 and plays an important role in L1 retrotransposition, possibly by affecting nuclear import of L1.

Discussion

Our data now provide an additional mechanistic context for our earlier report that miRs have adopted part of the role of piRNA in somatic cells to function as genomic gatekeepers by directly repressing L1 retrotransposon mobilization (37). In addition, we show for the first time that a cellular factor (TNPO1) is involved in L1 mobilization by facilitating nuclear import of some L1–RNP complexes, thus gaining access to host DNA. Our results are in alignment with previous reports describing that TNPO1 functions in nuclear transport of cargoes, including viral proteins (42, 43), and suggest that mobile DNA elements such as L1 elements are part of TNPO1 cargoes. Furthermore, recent data by Macia *et al.* (15) demonstrate that L1 can efficiently transpose in non-dividing cells. We propose that TNPO1 may be involved in active nuclear import of L1–RNP complexes in all cells but may be crucial for L1 mobilization in non-dividing cells such as neurons. It is possible that TNPO1 functions in a similar fashion during L1–RNP nuclear import, as TNPO3 has been demonstrated

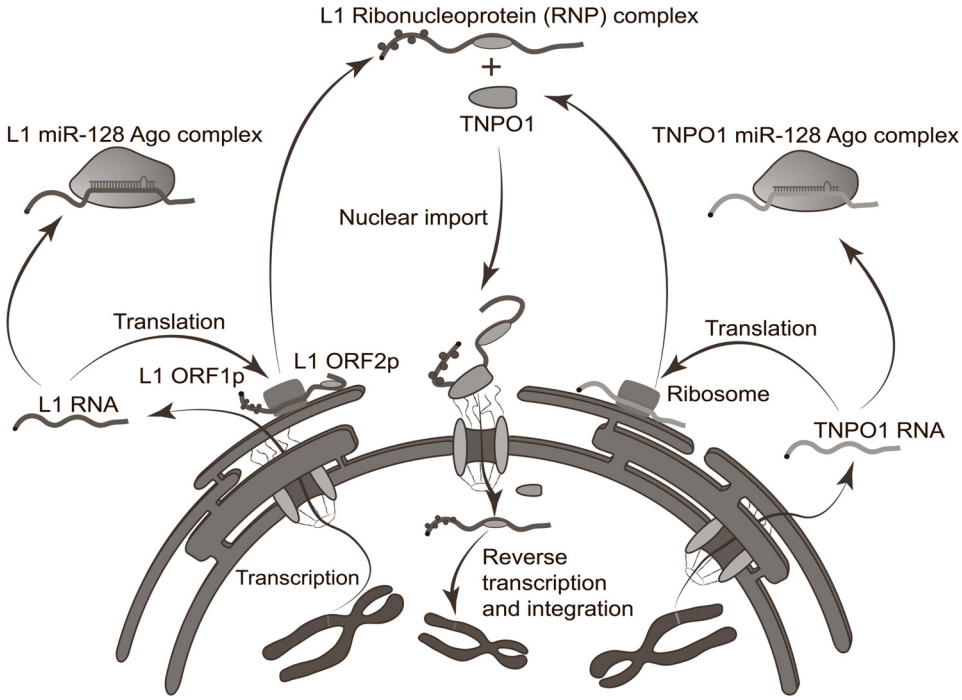

Figure 6. miR-128 regulates L1 retrotransposition by a dual mechanism. Shown is a schematic of miR-128–induced repression of L1 retrotransposition and genomic integration. miR-128 inhibits L1 activity by directly targeting L1 RNA as well as indirectly by repressing the levels of the cellular co-factor TNPO1, on which L1 is dependent for nuclear import and replication.

to assist with nuclear import of the preintegration complex of HIV-1 (53–59).

In summary, we propose a model for miR-128–induced L1 repression in which miR-128 acts by directly targeting L1 RNA (37) as well as indirectly reducing L1 mobilization by repressing a cellular factor involved in nuclear import of some L1–RNP complex (TNPO1) (Fig. 6). We speculate that a dual mechanism helps secure L1 restriction and, thus, L1-induced retrotransposition and genomic integration in somatic cells.

Interestingly, both TNPO1 and L1 ORF1p independently been found previously to interact with the heterogeneous nuclear ribonucleoprotein A1 (hnRNPA1), which contains NLSs required for shuttling between the cytoplasm and the nucleus (43, 48, 50–52, 61, 64, 65). We have now obtained results that support the idea that TNPO1 and ORF1p are also binding partners, either directly or through an RNA bridge (L1 RNA), suggesting a possible scenario in which nuclear import of the L1–RNP complex is assisted through ORF1p, TNPO1, and hnRNPA1 interactions. Another possible scenario is that ORF1p and/or ORF2p could be direct cargoes of TPNO1. Although a PY-NLS relies on structure, there is a weak consensus based on characterized motifs (R/H/KX^{2}-^{5}PY). Interestingly, both proteins contain PY motifs within the protein sequence, which fits the consensus (perfectly for ORF1p and partly for ORF2p). Future studies will determine whether these motifs are critical for L1 retrotransposition and binding to TPNO1.

All TNPO family proteins (TNPO1, TNPO2, and TNPO3) function in nuclear import (48, 50–52, 66–68). Interestingly, miR-128 harbors predicted binding sites in all three TNPO mRNAs, and our preliminary results show that miR-128 down-regulates the expression levels of TNPO1, TNPO2, and TNPO3 mRNAs. This finding has important implications, as TNPO3 is a demonstrated cellular co-factor on which HIV-1 is dependent for nuclear import of HIV-1 and viral replication (55–59). We anticipate that miR-128–induced TNPO3 repression could have significant effects on the viral life cycle of HIV-1.

Furthermore, miR-128 has been demonstrated previously to function as a tumor suppressor by inhibition of stemness and epithelial-to-mesenchymal transition through the regulation of target mRNAs, including BMI-1, Nanog, HIF-1, VEGF, TGFBR1, and EGFR (69–74). We predict that restriction of L1 insertions is another mechanism by which miR-128 plays a role in inhibiting tumor initiation and tumor cell progression.

Finally, it is interesting to note that the brain expresses ~70% of all mature miRs, that miR-128 is highly enriched in the brain compared with other human tissue (75, 76), and that L1 retrotransposition, surprisingly, has been found to be derepressed in neuronal progenitors, leading to somatic brain mosaicism and enhanced plasticity (77, 78). These finding suggest a potentially important role for miR-128 in the regulation of genomic instability and plasticity in the human brain.

In conclusion, our results show that increased miR-128 expression reduces nuclear import of L1 (ORF1p) and significantly inhibits L1 mobilization; up-regulation of TNPO1, a direct and functional target of miR-128, can markedly enhance levels of nuclear L1 (ORF1p) and *de novo* L1 retrotransposition. This newly identified miR-128/TNPO1 module provides a new avenue to an understanding of the L1 life cycle, especially how some L1–RNP complexes may access host DNA independently of cell division. Finally, the fact that TNPO1 can partially rescue the miR-128 inhibitory effect suggests that miR-128 may

repress additional cellular factors on which L1 is dependent for optimal genomic mobilization.

Experimental procedures

Cell culture

All cells were cultured at 37 °C and 5% CO_2. HeLa cells (CCL-2, ATCC) were cultured in Eagle's minimum essential medium (SH3024401, Hyclone) supplemented with 10% HI-FBS (FB-02, Omega Scientific), 5% Glutamax (35050-061, Thermo Fisher), 3% HEPES (15630-080, Thermo Fisher), and 1% Normocin (ant-nr-1, Invivogen). Tera-1 cells (HTB-105, ATCC) were cultured in McCoy's 5A (16600-082, Thermo Fisher) supplemented with 20% Cosmic Serum (SH3008702, Fisher Sci), and 1% Normocin (ant-nr-1, Invivogen). 293T cells (CRL-3216, ATCC) were cultured in DMEM supplemented with 10% HI-FBS (FB-02, Omega Scientific), 5% Glutamax (35050-061, Lifetech) and 1% Normocin (ant-nr-1, Invivogen). IMR90–1 cells were cultured in Nutristem complete medium (Stemgent). All cell lines were routinely tested for mycoplasma contamination.

Transfection and transduction of miRs

Opti-MEM (31985070, Thermo Fisher) and Lipofectamine RNAiMax (13778, Thermo Fisher) were used according to the instructions of the manufacturer to complex and transfect 20 μM miR-128 mimic or anti-miR-128 (C-301072-01 and IH-301072-02, respectively; Dharmacon) into cells. pJM101/L1-expressing plasmid was co-transfected with miR-128 mimic or anti-miR-128 into cells using Opti-MEM and Lipofectamine RNAiMax transfection reagent. Opti-MEM and Lipofectamine LTX with Plus reagent (15338030, Thermo Fisher) were used to complex and transfect 1 μg of FL-Control or FL-TNPO1 plasmid along with 0.5 μg of PhiC31 integrase plasmid according to the instructions of the manufacturer. Vesicular stomatitis virus G glycoprotein (VSVG)–pseudotyped lentiviral vectors were made by transfecting 0.67 μg of pMD2-G (12259, Addgene), 1.297 μg of pCMV-DR8.74 (8455, Addgene), and 2 μg of mZIP-miR-128, mZIP-anti-miR-128, pLKO-shControl, or pLKO-shTNPO1 (transfer plasmid) into 293T cells using Lipofectamine LTX with Plus reagent (15338030, Thermo Fisher). Virus-containing supernatant was collected 48 h and 96 h post-transfection. Viral supernatants were concentrated using PEG-it virus precipitation solution (LV810A-1) according to the instructions of the manufacturer. Cells were transduced with high-titer virus using Polybrene (sc-134220, Santa Cruz Biotechnology) and spinfection (800 × *g* at 32 °C for 30 min). Transduced cells were then incubated for 48 h at 37 °C and 5% CO_2. Cells were selected for 7 days using 3 μg/ml Puromycin. Stable lines were maintained in 3 μg/ml Puromycin.

RNA extraction and quantification of mRNAs

RNA was extracted using TRIzol (15596-018, Thermo Fisher) and the Direct-zol RNA isolation kit (R2070, Zymo Research). cDNA was made with a high-capacity cDNA reverse transcription kit (4368813, Thermo Fisher). mRNA levels were analyzed by qRT-PCR using SYBR Green (Thermo Fisher) or Forget-me-not qPCR Master Mix (Biotium) relative to the β-2-microglobulin (B2m) housekeeping gene and processed using the $\Delta\Delta C_t$ method.

Immunofluorescence

Cells were fixed with 4% paraformaldehyde (Sigma-Aldrich) and blocked with 10% goat serum (Thermo Fisher) + 0.1% Triton X-100 (Thermo Fisher). Anti-HA antibody was used 1:500 (C29F4, Cell Signaling Technology) and incubated for 24 h at 4 °C. Secondary goat anti-rabbit antibody conjugated to a488 (non-GFP–expressing cells) or a568 (for GFP–expressing cells) was used at 1:500. Slides were mounted with Vectashield containing DAPI counterstain (H-1200, Vector Laboratories). Images were acquired with a Zeiss LSM 700 confocal microscope in the Optical Biology Core at University of California Irvine. Co-localization of ORF1p-HA with the nucleus was calculated as follows: percent L1 ORF1p in the nucleus = (L1 ORF1p signal co-localized with nucleus / total L1 ORF1p signal) × 100. CellProfiler software (47) was utilized to automatically segment nuclei and determine the area of positive staining for L1 ORF1p, the area of positive staining for nuclei (DAPI), and the co-localized area of L1 ORF1p and nuclear staining. The amount of ORF1p in control nuclei was set to 100%, and the levels in the experimental nuclei are shown as a percentage of the controls.

qPCR screen for additional cellular targets of miR-128

As part of an effort to incorporate authentic research experiences into undergraduate laboratories at University of California Irvine, a basic screen to identify bioinformatically determined cellular targets of miR-128 was performed. Briefly, HeLa cells were transfected with 60 pmol of miR control or miR-128 mimics (GE Dharmacon) using Dharmafect1 (Thermo Fisher). After 24 h, cells were transfected a second time and incubated for another 24 h, after which cells were pelleted and snap-frozen in LN2. Control or miR-128–transfected pellets were provided to undergraduate students who isolated RNA and made cDNA using the GeneJET RNA purification kit (Thermo Fisher). qPCR was performed using student-designed primers to detect bioinformatically defined targets of miR-128 (Targetscan, Pictar). Graduate students further tested differentially expressed targets in independent biological replicates.

Site-directed mutagenesis

The reverse transcriptase–incompetent PJM101/L1 plasmid was made using the Q5 site-directed mutagenesis kit (E0554S, New England Biolabs) and the mutation strategy described in Morrish *et al.* (45), where D702A mutation in L1 ORF2 resulted in an incompetent reverse transcriptase.

Cloning

The ORF1-HA gene was generated by PCR on DNA from the plasmid pJM101/L1 (ORF1). To generate the ORF1-HA insert, we used the sense ORF1-HA primer 5′-GCCTAAGATCTA-GGTACCACCATGGGGAAAAAACAGAACAGAAAAAC-3′ and antisense ORF1-HA primer 5′-GTATCTTATCATGT-CTGGCCAGCTAGC*TTAGGCGTAGTCGGGCACGTCGT-AGGGGTAGCC*CATTTTGGCATGATTTTGCAGCG-3′ (the HA tag is shown in *italics*). All amplicons were generated

using the Phusion High-Fidelity PCR Kit (New England Biolabs) according to the protocol of the manufacturer. The amplicons were cloned into the expression vector pExpress-mUKG-MH1 by replacing the mUKG insert with the amplicon. For the generation of the plasmid backbone, the vector was cut by NcoI and NheI, and the insert was cloned into the backbone by using the cold fusion kit (SBI) according to the protocol of the manufacturer. The resulting plasmid, pExpress-ORF1-HA-MH1, was amplified in *Escherichia coli* and validated by sequencing.

TNPO1 shRNA was designed using the RNAi Consortium (https://www.broadinstitute.org/rnai/public/)[3] using clone TRCN0000382164 and cloned into the pLKO.1 puro backbone (Addgene, 8453). The pLKO shGFP control plasmid was preassembled (Addgene, 30323).

For the TNPO1 full-length clone, we modified the plasmid pFC-PGK-MCS-pA-EF1-GFP-T2A-Puro (SBI, backbone) by replacing the PGK with a CMV promoter. The CMV promoter provides strong and robust expression in most cell types. The CMV promoter was amplified by PCR from the phiC31 integrase expression plasmid (SBI). To generate the CMV promoter insert, we used the sense CMV primer 5′-CTAGAACTAGTTATTAATAGTAATCAATTACGGGGTC-3′ and antisense CMV primer 5′-GATATCGGATCCACCGGTACCAAGCTTAAGTTTAAAC-3′. The insert and the backbone of the plasmid were cut by XbaI and BamHI and purified by an agarose gel. The insert and backbone were ligated together using the quick ligation kit (New England Bioloabs) and transformed. The resulting plasmid pFC-CMV-MCS-pA-EF-1-GFP-T2A-Puro-MH1 was verified by sequencing.

For the cloning of the full-length TNPO1 mRNA expression clone (FL-TNPO1), we isolated total RNA from A549 and HeLa cells. 20 ng of the total RNA was reverse-transcribed using a poly(dT) primer. For amplification of the TNPO1 gene, we used the sense TNPO1 (5′-TTTAAACTTAAGCTTGGTACCGGTGGATCCGCCACCATGGAGTATGAGTGGAAACCTGAC-3′) and antisense TNPO1 (5′-GATTAAACACCATAAAAAGCTGCA-3′). The 3′ UTR of the gene that exhibits the binding site for miR-128 was split into four fragments. For the four parts, the following primers were used: part 1, 3′ UTR primer sense 1 (5′-GGAAGGGTAAACCAGTAGGGAATA-3′) and 3′ UTR antisense 1 (5′-GGGTTAACTTAACAAGGATTTATTCAC-3′); part 2, 3′ UTR primer sense 2 (5′-CTGTGAATAAATCCTTGTTAAGTTAAC-3′) and 3′ UTR antisense 2 (5′-GTAAACACTGACCTCCTGAGGTTCCTA-3′); part 3, 3′ UTR primer sense 3 (5′-GTAGGAACCTCAGGAGGTCAGTGTTTA-3′) and 3′ UTR antisense 3 (5′-GGGATACAAACCACAATGAACAAT-3′); part 4, 3′ UTR primer sense 4 (5′-CAATTGTTCATTGTGGTTTGTATC-3′) and (5′-GGCAACTAGAAGGCACAGTCGATCGATTATAGTTAAACAACTTTATTAACATAGTCAAGC-3′). All amplicons were generated using the Phusion High-Fidelity PCR Kit (New England Biolabs) according to the protocol of the manufacturer. The fragments were assembled step-wise by using the cold fusion kit (SBI) and cloned into the pFC-CMV-MCS-pA-EF-1-GFP-T2A-Puro-MH1 BamHI/ClaI linearized backbone by cold fusion. The resulting plasmid (pFC-CMV-TNPO1-pA-EF-1-GFP-T2A-Puro-MH1) was verified by sequencing. FL-Control is an empty vector.

[3] Please note that the JBC is not responsible for the long-term archiving and maintenance of this site or any other third party–hosted site.

Colony formation assay

Stable HeLa lines expressing miR control, miR-128, anti-miR-128, shControl, shTNPO1, FL-Control, and FL-TNPO1 were plated at 5×10^5 cells/well of a 6-well plate and incubated for 24 h. Cells were then transfected with 0.5 μg of pJM101/L1RP or pJM101/L1RP RT (containing the neomycin resistance retrotransposition indicator cassette) per well using X-treme Gene HP DNA transfection reagent (06366236001, Roche) according to the instructions of the manufacturer. Cells were incubated for 24 h, followed by a medium change without antibiotics. 48 h after transfection, selection by daily medium changes containing 500 μg/ml G418 (ant-gn-1, Invivogen) were initiated. Daily medium changes were continued until all cells died in the negative control (untransfected HeLa cells). Neomycin-resistant colonies were fixed with cold 1:1 methanol:acetone and then visualized using May–Grunwald (ES-3410, Thermo Fisher) and Jenner–Giemsa staining kits (ES-8150, Thermo Fisher) according to the protocol of the manufacturer.

Luciferase assays

WT TNPO1 binding site 1, WT TNPO1 binding site 2, WT TNPO1 binding site 3, mutated binding site 1, or positive control (complete complementary) (see Fig. 2, *A* and *C*) sequences were cloned into a Dual-Luciferase reporter plasmid (pEZX-MT05, Genecopoeia). 3×10^5 HeLa cells were transfected at the same time as seeding with 0.8 μg of reporter plasmid (WT, mutated, Pos) and 20 nM miR-128 mimic (Dharmacon) or control mimic (Dharmacon) using Attractene transfection reagent (301005, Qiagen) according to the instructions of the manufacturer. Cells were incubated for 48 h at 37 °C and 5% CO_2 without medium change. Relative *Gaussia* luciferase and secreted alkaline phosphatase were determined using the Secrete-Pair Dual Luminescence Assay Kit (SPDA-D010, Genecopoeia) in technical triplicates from collected supernatant. Relative *Gaussia* luciferase was detected by a Tecan Infinite F200 Pro microplate reader.

Fractionation

Nuclear and cytoplasmic fractions were isolated using a protein and RNA isolation system or PARIS kit (AM1921, Thermo Fisher) according to the instructions of the manufacturer 48 h after transfection. Both RNA and protein were isolated from the same biological sample (shControl, shTNPO1, FL-Control, and FL-TNPO1) and used for qRT-PCR and corresponding Western blot analysis, respectively.

Immunoprecipitation

Transfected cells were lysed in radioimmune precipitation assay buffer and protease inhibitors on ice for 15 min. Lysate was cleared by centrifuging at 13,000 rpm (maximum speed, tabletop centrifuge) for 15 min at 4 °C. Supernatant was collected, and a portion was reserved as input for Western blot analysis. The remaining immunoprecipitate was mixed with protein G beads (New England Biolabs) and 5 μg of anti-HA

antibody and incubated on a rotator for 24 h at 4 °C. Beads were separated using a magnetic rack and washed four times with PBS. Beads were then boiled for 5 min at 95 °C in 4× protein loading dye (+SDS). Beads were separated, and supernatant containing the immunoprecipitated proteins was used for Western blot analysis.

Western blot analysis

Mouse anti-human L1 ORF1p (MABC1152 clone 4H1) from Millipore was used at 1:1000. Rabbit anti-human L1 ORF1p antibody custom-generated by Genscript against ORF1p and validated by ELISA was used at 1:1000. The Western blot analysis of Genscript antibody was initially cross-checked by a custom generated anti-human L1 ORF1p antibody (kindly provided by G. Schumann). Rabbit anti-HA antibody to detect HA-tagged L1 ORF1p (C29F4, Cell Signaling Technology) was used at 1:5000, mouse anti-TNPO1 antibody was used at 1:2000 (ab10303, Abcam), rabbit anti-hnRNPA1 antibody was used at 1:2000 (K350, Cell Signaling Technology). Anti-α-tubulin antibody (ab4074, Abcam) diluted 1:5000 and anti-GAPDH antibody (^{14}C10, Cell Signaling Technology) diluted 1:3000 were used as loading controls; validation can be found on the websites of the manufacturers. Secondary HRP-conjugated anti-rat (ab102172, Abcam), HRP-conjugated anti-rabbit (GE Healthcare), and HRP-conjugated anti-mouse (GE Healthcare) antibodies were used at 1:5000. ECL substrate (32106, Thermo Fisher) was added and visualized on a Bio-Rad ChemiDoc imager. Because many proteins were similar in size, blots were not cut but developed sequentially. After developing, each blot was washed three times in 1× TBST (TBS (BP24711, FisherSci) and 0.05% Tween 20 (BP337-500, FisherSci)) prior to incubation with the next primary antibody.

Argonaute RNA immunopurification (Ago RIP)

Immunopurification of Argonaute from HeLa cell extracts was performed using the 4F9 antibody (Santa Cruz Biotechnology) as described previously (79, 80). Briefly, 10-mm plates of 80% confluent cultured cells were washed with buffer A (20 mM Tris-HCl (pH 8.0), 140 mM KCl, and 5 mM EDTA) and lysed in 200 μl of buffer 2XB (40 mM Tris-HCl (pH 8.0), 280 mM KCl, 10 mM EDTA, 1% Nonidet P-40, 0.2% deoxycholate, and 2× Halt protease inhibitor mixture (Pierce)), 200 units/ml RNaseout (Thermo Fisher), and 1 mM DTT. The protein concentration was adjusted across samples with buffer B (20 mM Tris-HCl (pH 8.0), 140 mM KCl, 5 mM EDTA (pH 8.0), 0.5% Nonidet P-40, 0.1% deoxycholate, 100 units/ml RNaseout (Thermo Fisher), 1 mM DTT, and 1× Halt protease inhibitor mixture (Pierce)). Lysates were centrifuged at 16,000 × *g* for 15 min at 4 °C, and supernatants were incubated with 10–20 μg of 4F9 antibody conjugated to epoxy magnetic beads (M-270 Dynabeads, Thermo Fisher) for 2 h at 4 °C with gentle rotation (nutator). The beads, following magnetic separation, were washed three times for 5 min with 2 ml of buffer C (20 mM Tris-HCl (pH 8.0), 140 mM KCl, 5 mM EDTA (pH 8.0), 40 units/ml RNaseout (Thermo Fisher), 1 mM DTT, and 1× Halt protease inhibitor mixture (Pierce)). Following immunopurification, RNA was extracted using miRNeasy kits (Qiagen) following the recommendations of the manufacturer, and qPCR was performed using custom probes/primers for the TNPO1 mRNA transcript and Forget-me-not qPCR Master Mix (Biotium). Results were normalized to their inputs and shown as "corrected" values as a proxy for Ago immunopurification efficiency.

Statistical analysis

Student's t tests were used to calculate two-tailed *p* values, and data are displayed as means ± S.E. of technical replicates or independent biological replicates (*n*) as indicated.

Author contributions—A. I. performed the majority of experiments demonstrating that miR-128 targets TNPO1 and that miR-128-induced L1 restriction is partly dependent on TNPO1, helped generate the first version of the figures, and gave input on the manuscript. E. A. S. performed colony formation assays and cross-validated ORF1p antibodies. D. G. Z. performed the Ago RNA immunoprecipitations. M. H. generated the miR-128–resistant L1 and TNPO1 overexpressing plasmids. I. D. performed some experiments, generated the final figures, and commented on the manuscript. P. K. directed the evaluation of miR-128 targets in the laboratory class module. I. M. P. performed some experiments, directed all experiments and figure design, and wrote the manuscript. All authors reviewed the results and approved the final version of the manuscript.

Acknowledgments—We thank the undergraduate students involved in the miR-128 screen effort as part of laboratory class at University of California, Irvine and Y. Castuera and D. Jury for laboratory assistance with quantifying results. We also thank J. Moran (University of Michigan Medical School, Ann Arbor, MI) and M. An (Washington State University, Pullman, WA) for generously sharing the pJM101/L1 and pWA355 plasmids and A. Mortazavi (University of California, Irvine) for generously sharing reagents and support.

References

1. Lander, E. S., Linton, L. M., Birren, B., Nusbaum, C., Zody, M. C., Baldwin, J., Devon, K., Dewar, K., Doyle, M., FitzHugh, W., Funke, R., Gage, D., Harris, K., Heaford, A., Howland, J., *et al.* (2001) Initial sequencing and analysis of the human genome. *Nature* **409,** 860–921
2. Moran, J. V., Holmes, S. E., Naas, T. P., DeBerardinis, R. J., Boeke, J. D., and Kazazian, H. H., Jr. (1996) High frequency retrotransposition in cultured mammalian cells. *Cell* **87,** 917–927
3. Scott, A. F., Schmeckpeper, B. J., Abdelrazik, M., Comey, C. T., O'Hara, B., Rossiter, J. P., Cooley, T., Heath, P., Smith, K. D., and Margolet, L. (1987) Origin of the human L1 elements: proposed progenitor genes deduced from a consensus DNA sequence. *Genomics* **1,** 113–125
4. Speek, M. (2001) Antisense promoter of human L1 retrotransposon drives transcription of adjacent cellular genes. *Mol. Cell. Biol.* **21,** 1973–1985
5. Swergold, G. D. (1990) Identification, characterization, and cell specificity of a human LINE-1 promoter. *Mol. Cell. Biol.* **10,** 6718–6729
6. Yang, N., and Kazazian, H. H., Jr. (2006) L1 retrotransposition is suppressed by endogenously encoded small interfering RNAs in human cultured cells. *Nat. Struct. Mol. Biol.* **13,** 763–771
7. Kolosha, V. O., and Martin, S. L. (1997) *In vitro* properties of the first ORF protein from mouse LINE-1 support its role in ribonucleoprotein particle formation during retrotransposition. *Proc. Natl. Acad. Sci. U.S.A.* **94,** 10155–10160
8. Feng, Q., Moran, J. V., Kazazian, H. H., Jr, and Boeke, J. D. (1996) Human L1 retrotransposon encodes a conserved endonuclease required for retrotransposition. *Cell* **87,** 905–916
9. Mathias, S. L., Scott, A. F., Kazazian, H. H., Jr, Boeke, J. D., and Gabriel, A. (1991) Reverse transcriptase encoded by a human transposable element. *Science* **254,** 1808–1810

10. Kleckner, N. (1990) Regulation of transposition in bacteria. *Annu. Rev. Cell Biol.* **6,** 297–327
11. Luan, D. D., Korman, M. H., Jakubczak, J. L., and Eickbush, T. H. (1993) Reverse transcription of R2Bm RNA is primed by a nick at the chromosomal target site: a mechanism for non-LTR retrotransposition. *Cell* **72,** 595–605
12. Kubo, S., Seleme, M. C., Soifer, H. S., Perez, J. L., Moran, J. V., Kazazian, H. H., Jr., and Kasahara, N. (2006) L1 retrotransposition in nondividing and primary human somatic cells. *Proc. Natl. Acad. Sci. U.S.A.* **103,** 8036–8041
13. Shi, X., Seluanov, A., and Gorbunova, V. (2007) Cell divisions are required for L1 retrotransposition. *Mol. Cell. Biol.* **27,** 1264–1270
14. Xie, Y., Mates, L., Ivics, Z., Izsvák, Z., Martin, S. L., and An, W. (2013) Cell division promotes efficient retrotransposition in a stable L1 reporter cell line. *Mobile DNA* **4,** 10
15. Macia, A., Widmann, T. J., Heras, S. R., Ayllon, V., Sanchez, L., Benkaddour-Boumzaouad, M., Muñoz-Lopez, M., Rubio, A., Amador-Cubero, S., Blanco-Jimenez, E., Garcia-Castro, J., Menendez, P., Ng, P., Muotri, A. R., Goodier, J. L., and Garcia-Perez, J. L. (2017) Engineered LINE-1 retrotransposition in nondividing human neurons. *Genome Res.* **27,** 335–348
16. Nigumann, P., Redik, K., Mätlik, K., and Speek, M. (2002) Many human genes are transcribed from the antisense promoter of L1 retrotransposon. *Genomics* **79,** 628–634
17. Perepelitsa-Belancio, V., and Deininger, P. (2003) RNA truncation by premature polyadenylation attenuates human mobile element activity. *Nat. Genet.* **35,** 363–366
18. Moran, J. V., DeBerardinis, R. J., and Kazazian, H. H., Jr. (1999) Exon shuffling by L1 retrotransposition. *Science* **283,** 1530–1534
19. Kazazian, H. H., Jr. (2004) Mobile elements: drivers of genome evolution. *Science* **303,** 1626–1632
20. Beck, C. R., Garcia-Perez, J. L., Badge, R. M., and Moran, J. V. (2011) LINE-1 elements in structural variation and disease. *Annu. Rev. Genomics Hum. Genet.* **12,** 187–215
21. Cordaux, R., and Batzer, M. A. (2009) The impact of retrotransposons on human genome evolution. *Nat. Rev. Genet.* **10,** 691–703
22. Hancks, D. C., and Kazazian, H. H., Jr. (2012) Active human retrotransposons: variation and disease. *Curr. Opin. Genet. Dev.* **22,** 191–203
23. Shukla, R., Upton, K. R., Muñoz-Lopez, M., Gerhardt, D. J., Fisher, M. E., Nguyen, T., Brennan, P. M., Baillie, J. K., Collino, A., Ghisletti, S., Sinha, S., Iannelli, F., Radaelli, E., Dos Santos, A., Rapoud, D., *et al.* (2013) Endogenous retrotransposition activates oncogenic pathways in hepatocellular carcinoma. *Cell* **153,** 101–111
24. Aravin, A. A., Sachidanandam, R., Girard, A., Fejes-Toth, K., and Hannon, G. J. (2007) Developmentally regulated piRNA clusters implicate MILI in transposon control. *Science* **316,** 744–747
25. Kuramochi-Miyagawa, S., Watanabe, T., Gotoh, K., Totoki, Y., Toyoda, A., Ikawa, M., Asada, N., Kojima, K., Yamaguchi, Y., Ijiri, T. W., Hata, K., Li, E., Matsuda, Y., Kimura, T., Okabe, M., *et al.* (2008) DNA methylation of retrotransposon genes is regulated by Piwi family members MILI and MIWI2 in murine fetal testes. *Genes Dev.* **22,** 908–917
26. Tsutsumi, Y. (2000) Hypomethylation of the retrotransposon LINE-1 in malignancy. *Jpn. J. Clin. Oncol.* **30,** 289–290
27. Smith, Z. D., Chan, M. M., Mikkelsen, T. S., Gu, H., Gnirke, A., Regev, A., and Meissner, A. (2012) A unique regulatory phase of DNA methylation in the early mammalian embryo. *Nature* **484,** 339–344
28. Chalitchagorn, K., Shuangshoti, S., Hourpai, N., Kongruttanachok, N., Tangkijvanich, P., Thong-ngam, D., Voravud, N., Sriuranpong, V., and Mutirangura, A. (2004) Distinctive pattern of LINE-1 methylation level in normal tissues and the association with carcinogenesis. *Oncogene* **23,** 8841–8846
29. Wissing, S., Muñoz-Lopez, M., Macia, A., Yang, Z., Montano, M., Collins, W., Garcia-Perez, J. L., Moran, J. V., and Greene, W. C. (2012) Reprogramming somatic cells into iPS cells activates LINE-1 retroelement mobility. *Hum. Mol. Genet.* **21,** 208–218
30. Koito, A., and Ikeda, T. (2011) Intrinsic restriction activity by AID/APOBEC family of enzymes against the mobility of retroelements. *Mob. Genet. Elements* **1,** 197–202
31. Bogerd, H. P., Wiegand, H. L., Doehle, B. P., and Cullen, B. R. (2007) The intrinsic antiretroviral factor APOBEC3B contains two enzymatically active cytidine deaminase domains. *Virology* **364,** 486–493
32. Ambros, V. (2004) The functions of animal microRNAs. *Nature* **431,** 350–355
33. Heras, S. R., Macias, S., Plass, M., Fernandez, N., Cano, D., Eyras, E., Garcia-Perez, J. L., and Cáceres, J. F. (2013) The microprocessor controls the activity of mammalian retrotransposons. *Nat. Struct. Mol. Biol.* **20,** 1173–1181
34. Bartel, D. P. (2004) MicroRNAs: genomics, biogenesis, mechanism, and function. *Cell* **116,** 281–297
35. Bartel, D. P. (2009) MicroRNAs: target recognition and regulatory functions. *Cell* **136,** 215–233
36. Fabian, M. R., Sonenberg, N., and Filipowicz, W. (2010) Regulation of mRNA translation and stability by microRNAs. *Annu. Rev. Biochem.* **79,** 351–379
37. Hamdorf, M., Idica, A., Zisoulis, D. G., Gamelin, L., Martin, C., Sanders, K. J., and Pedersen, I. M. (2015) miR-128 represses L1 retrotransposition by binding directly to L1 RNA. *Nat. Struct. Mol. Biol.* **22,** 824–831
38. Vella, M. C., Choi, E. Y., Lin, S. Y., Reinert, K., and Slack, F. J. (2004) The *C. elegans* microRNA let-7 binds to imperfect let-7 complementary sites from the lin-41 3′UTR. *Genes Dev.* **18,** 132–137
39. Lin, C. W., Chang, Y. L., Chang, Y. C., Lin, J. C., Chen, C. C., Pan, S. H., Wu, C. T., Chen, H. Y., Yang, S. C., Hong, T. M., and Yang, P. C. (2013) MicroRNA-135b promotes lung cancer metastasis by regulating multiple targets in the Hippo pathway and LZTS1. *Nat. Commun.* **4,** 1877
40. Kent, O. A., Fox-Talbot, K., and Halushka, M. K. (2013) RREB1 repressed miR-143/145 modulates KRAS signaling through downregulation of multiple targets. *Oncogene* **32,** 2576–2585
41. Le, M. T., Xie, H., Zhou, B., Chia, P. H., Rizk, P., Um, M., Udolph, G., Yang, H., Lim, B., and Lodish, H. F. (2009) MicroRNA-125b promotes neuronal differentiation in human cells by repressing multiple targets. *Mol. Cell. Biol.* **29,** 5290–5305
42. Twyffels, L., Gueydan, C., and Kruys, V. (2014) Transportin-1 and Transportin-2: protein nuclear import and beyond. *FEBS Lett.* **588,** 1857–1868
43. Kimura, M., Kose, S., Okumura, N., Imai, K., Furuta, M., Sakiyama, N., Tomii, K., Horton, P., Takao, T., and Imamoto, N. (2013) Identification of cargo proteins specific for the nucleocytoplasmic transport carrier transportin by combination of an *in vitro* transport system and stable isotope labeling by amino acids in cell culture (SILAC)-based quantitative proteomics. *Mol. Cell. Proteomics* **12,** 145–157
44. Wei, W., Gilbert, N., Ooi, S. L., Lawler, J. F., Ostertag, E. M., Kazazian, H. H., Boeke, J. D., and Moran, J. V. (2001) Human L1 retrotransposition: cis preference versus trans complementation. *Mol. Cell. Biol.* **21,** 1429–1439
45. Morrish, T. A., Garcia-Perez, J. L., Stamato, T. D., Taccioli, G. E., Sekiguchi, J., and Moran, J. V. (2007) Endonuclease-independent LINE-1 retrotransposition at mammalian telomeres. *Nature* **446,** 208–212
46. Carpenter, A. E., Jones, T. R., Lamprecht, M. R., Clarke, C., Kang, I. H., Friman, O., Guertin, D. A., Chang, J. H., Lindquist, R. A., Moffat, J., Golland, P., and Sabatini, D. M. (2006) CellProfiler: image analysis software for identifying and quantifying cell phenotypes. *Genome Biol.* **7,** R100
47. Agarwal, V., Bell, G. W., Nam, J. W., and Bartel, D. P. (2015) Predicting effective microRNA target sites in mammalian mRNAs. *eLife* **4,** 10.7554/eLife.05005
48. Nakielny, S., Siomi, M. C., Siomi, H., Michael, W. M., Pollard, V., and Dreyfuss, G. (1996) Transportin: nuclear transport receptor of a novel nuclear protein import pathway. *Exp. Cell Res.* **229,** 261–266
49. Lee, B. J., Cansizoglu, A. E., Süel, K. E., Louis, T. H., Zhang, Z., and Chook, Y. M. (2006) Rules for nuclear localization sequence recognition by karyopherin β 2. *Cell* **126,** 543–558
50. Pollard, V. W., Michael, W. M., Nakielny, S., Siomi, M. C., Wang, F., and Dreyfuss, G. (1996) A novel receptor-mediated nuclear protein import pathway. *Cell* **86,** 985–994
51. Fridell, R. A., Truant, R., Thorne, L., Benson, R. E., and Cullen, B. R. (1997) Nuclear import of hnRNP A1 is mediated by a novel cellular cofactor related to karyopherin-β. *J. Cell Sci.* **110,** 1325–1331

52. Bonifaci, N., Moroianu, J., Radu, A., and Blobel, G. (1997) Karyopherin β2 mediates nuclear import of a mRNA binding protein. *Proc. Natl. Acad. Sci. U.S.A.* **94,** 5055–5060
53. Christ, F., Thys, W., De Rijck, J., Gijsbers, R., Albanese, A., Arosio, D., Emiliani, S., Rain, J. C., Benarous, R., Cereseto, A., and Debyser, Z. (2008) Transportin-SR2 imports HIV into the nucleus. *Curr. Biol.* **18,** 1192–1202
54. De Iaco, A., and Luban, J. (2011) Inhibition of HIV-1 infection by TNPO3 depletion is determined by capsid and detectable after viral cDNA enters the nucleus. *Retrovirology* **8,** 98
55. De Iaco, A., Santoni, F., Vannier, A., Guipponi, M., Antonarakis, S., and Luban, J. (2013) TNPO3 protects HIV-1 replication from CPSF6-mediated capsid stabilization in the host cell cytoplasm. *Retrovirology* **10,** 20
56. Krishnan, L., Matreyek, K. A., Oztop, I., Lee, K., Tipper, C. H., Li, X., Dar, M. J., Kewalramani, V. N., and Engelman, A. (2010) The requirement for cellular transportin 3 (TNPO3 or TRN-SR2) during infection maps to human immunodeficiency virus type 1 capsid and not integrase. *J. Virol.* **84,** 397–406
57. Maertens, G. N., Cook, N. J., Wang, W., Hare, S., Gupta, S. S., Öztop, I., Lee, K., Pye, V. E., Cosnefroy, O., Snijders, A. P., KewalRamani, V. N., Fassati, A., Engelman, A., and Cherepanov, P. (2014) Structural basis for nuclear import of splicing factors by human Transportin 3. *Proc. Natl. Acad. Sci. U.S.A.* **111,** 2728–2733
58. Valle-Casuso, J. C., Di Nunzio, F., Yang, Y., Reszka, N., Lienlaf, M., Arhel, N., Perez, P., Brass, A. L., and Diaz-Griffero, F. (2012) TNPO3 is required for HIV-1 replication after nuclear import but prior to integration and binds the HIV-1 core. *J. Virol.* **86,** 5931–5936
59. Lee, K., Ambrose, Z., Martin, T. D., Oztop, I., Mulky, A., Julias, J. G., Vandegraaff, N., Baumann, J. G., Wang, R., Yuen, W., Takemura, T., Shelton, K., Taniuchi, I., Li, Y., Sodroski, J., Littman, D. R., *et al.* (2010) Flexible use of nuclear import pathways by HIV-1. *Cell Host Microbe* **7,** 221–233
60. Neumann, M., Bentmann, E., Dormann, D., Jawaid, A., DeJesus-Hernandez, M., Ansorge, O., Roeber, S., Kretzschmar, H. A., Munoz, D. G., Kusaka, H., Yokota, O., Ang, L. C., Bilbao, J., Rademakers, R., Haass, C., and Mackenzie, I. R. (2011) FET proteins TAF15 and EWS are selective markers that distinguish FTLD with FUS pathology from amyotrophic lateral sclerosis with FUS mutations. *Brain* **134,** 2595–2609
61. Goodier, J. L., Cheung, L. E., and Kazazian, H. H., Jr. (2013) Mapping the LINE1 ORF1 protein interactome reveals associated inhibitors of human retrotransposition. *Nucleic Acids Res.* **41,** 7401–7419
62. Pedersen, I. M., Cheng, G., Wieland, S., Volinia, S., Croce, C. M., Chisari, F. V., and David, M. (2007) Interferon modulation of cellular microRNAs as an antiviral mechanism. *Nature* **449,** 919–922
63. Nathans, R., Chu, C. Y., Serquina, A. K., Lu, C. C., Cao, H., and Rana, T. M. (2009) Cellular microRNA and P bodies modulate host-HIV-1 interactions. *Mol. Cell* **34,** 696–709
64. Goodier, J. L., Zhang, L., Vetter, M. R., and Kazazian, H. H., Jr. (2007) LINE-1 ORF1 protein localizes in stress granules with other RNA-binding proteins, including components of RNA interference RNA-induced silencing complex. *Mol. Cell. Biol.* **27,** 6469–6483
65. Siomi, M. C., Eder, P. S., Kataoka, N., Wan, L., Liu, Q., and Dreyfuss, G. (1997) Transportin-mediated nuclear import of heterogeneous nuclear RNP proteins. *J. Cell Biol.* **138,** 1181–1192
66. Güttinger, S., Mühlhäusser, P., Koller-Eichhorn, R., Brennecke, J., and Kutay, U. (2004) Transportin2 functions as importin and mediates nuclear import of HuR. *Proc. Natl. Acad. Sci. U.S.A.* **101,** 2918–2923
67. Rebane, A., Aab, A., and Steitz, J. A. (2004) Transportins 1 and 2 are redundant nuclear import factors for hnRNP A1 and HuR. *RNA* **10,** 590–599
68. Xu, D., Farmer, A., and Chook, Y. M. (2010) Recognition of nuclear targeting signals by Karyopherin-β proteins. *Curr. Opin. Struct. Biol.* **20,** 782–790
69. Shi, Z. M., Wang, J., Yan, Z., You, Y. P., Li, C. Y., Qian, X., Yin, Y., Zhao, P., Wang, Y. Y., Wang, X. F., Li, M. N., Liu, L. Z., Liu, N., and Jiang, B. H. (2012) MiR-128 inhibits tumor growth and angiogenesis by targeting p70S6K1. *PLoS ONE* **7,** e32709
70. Zhang, Y., Chao, T., Li, R., Liu, W., Chen, Y., Yan, X., Gong, Y., Yin, B., Liu, W., Qiang, B., Zhao, J., Yuan, J., and Peng, X. (2009) MicroRNA-128 inhibits glioma cells proliferation by targeting transcription factor E2F3a. *J. Mol. Med.* **87,** 43–51
71. Masri, S., Liu, Z., Phung, S., Wang, E., Yuan, Y. C., and Chen, S. (2010) The role of microRNA-128a in regulating TGFβ signaling in letrozole-resistant breast cancer cells. *Breast Cancer Res. Treat.* **124,** 89–99
72. Qian, P., Banerjee, A., Wu, Z. S., Zhang, X., Wang, H., Pandey, V., Zhang, W. J., Lv, X. F., Tan, S., Lobie, P. E., and Zhu, T. (2012) Loss of SNAIL regulated miR-128-2 on chromosome 3p22.3 targets multiple stem cell factors to promote transformation of mammary epithelial cells. *Cancer Res.* **72,** 6036–6050
73. Jin, M., Zhang, T., Liu, C., Badeaux, M. A., Liu, B., Liu, R., Jeter, C., Chen, X., Vlassov, A. V., and Tang, D. G. (2014) miRNA-128 suppresses prostate cancer by inhibiting BMI-1 to inhibit tumor-initiating cells. *Cancer Res.* **74,** 4183–4195
74. Liu, J., Cao, L., Chen, J., Song, S., Lee, I. H., Quijano, C., Liu, H., Keyvanfar, K., Chen, H., Cao, L. Y., Ahn, B. H., Kumar, N. G., Rovira, I. I., Xu, X. L., van Lohuizen, M., *et al.* (2009) Bmi1 regulates mitochondrial function and the DNA damage response pathway. *Nature* **459,** 387–392
75. Sempere, L. F., Freemantle, S., Pitha-Rowe, I., Moss, E., Dmitrovsky, E., and Ambros, V. (2004) Expression profiling of mammalian microRNAs uncovers a subset of brain-expressed microRNAs with possible roles in murine and human neuronal differentiation. *Genome Biol.* **5,** R13
76. Fineberg, S. K., Kosik, K. S., and Davidson, B. L. (2009) MicroRNAs potentiate neural development. *Neuron* **64,** 303–309
77. Singer, T., McConnell, M. J., Marchetto, M. C., Coufal, N. G., and Gage, F. H. (2010) LINE-1 retrotransposons: mediators of somatic variation in neuronal genomes? *Trends Neurosci.* **33,** 345–354
78. Erwin, J. A., Marchetto, M. C., and Gage, F. H. (2014) Mobile DNA elements in the generation of diversity and complexity in the brain. *Nat. Rev. Neurosci.* **15,** 497–506
79. Hunter, S. E., Finnegan, E. F., Zisoulis, D. G., Lovci, M. T., Melnik-Martinez, K. V., Yeo, G. W., and Pasquinelli, A. E. (2013) Functional genomic analysis of the let-7 regulatory network in *Caenorhabditis elegans*. *PLoS Genet.* **9,** e1003353
80. Hogan, D. J., Vincent, T. M., Fish, S., Marcusson, E. G., Bhat, B., Chau, B. N., and Zisoulis, D. G. (2014) Anti-miRs competitively inhibit microRNAs in Argonaute complexes. *PLoS ONE* **9,** e100951